The Journal of Chemical Physics

A quantum Langevin equation approach for two-dimensional electronic spectra of coupled vibrational and electronic dynamics

Cite as: J. Chem. Phys. **154**, 154107 (2021); https://doi.org/10.1063/5.0042848
Submitted: 04 January 2021 . Accepted: 06 April 2021 . Published Online: 21 April 2021

Man Tou Wong, and **Yuan-Chung Cheng**

View Online Export Citation CrossMark

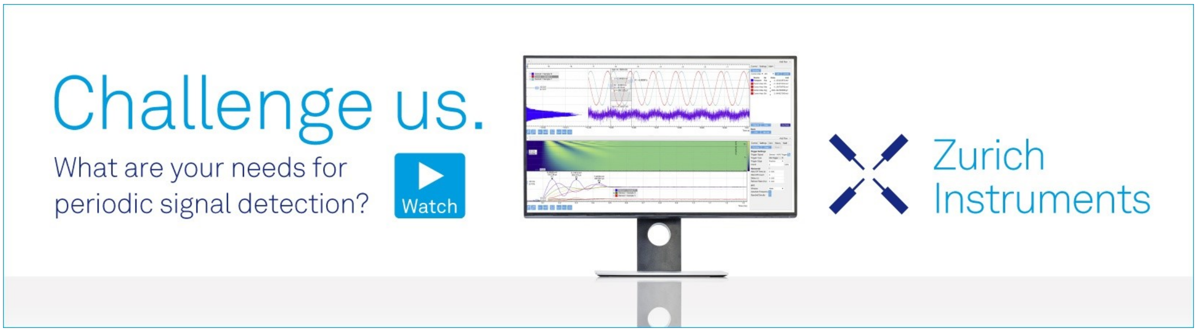

AIP Publishing

The Journal of Chemical Physics ARTICLE scitation.org/journal/jcp

A quantum Langevin equation approach for two-dimensional electronic spectra of coupled vibrational and electronic dynamics

Cite as: J. Chem. Phys. **154**, 154107 (2021); doi: 10.1063/5.0042848
Submitted: 4 January 2021 • Accepted: 6 April 2021 •
Published Online: 21 April 2021

View Online Export Citation CrossMark

Man Tou Wong and **Yuan-Chung Cheng**[a)]

AFFILIATIONS

Department of Chemistry and Center for Quantum Science and Engineering, National Taiwan University, Taipei City 106, Taiwan

Note: This paper is part of the JCP Special Topic on Coherent Multidimensional Spectroscopy.
[a)] **Author to whom correspondence should be addressed:** yuanchung@ntu.edu.tw

ABSTRACT

We present an efficient method to simulate two-dimensional (2D) electronic spectra of condensed-phase systems with an emphasis on treating quantum nuclear wave packet dynamics explicitly. To this end, we combine a quantum Langevin equation (QLE) approach for dissipation and a perturbative scheme to calculate three-pulse photon-echo polarizations based on wave packet dynamics under the influence of external fields. The proposed dynamical approach provides a consistent description of nuclear quantum dynamics, pulse-overlap effects, and vibrational relaxation, enabling simulations of 2D electronic spectra with explicit and non-perturbative treatment of coupled electronic–nuclear dynamics. We apply the method to simulate 2D electronic spectra of a displaced-oscillator model in the condensed phase and discuss the spectral and temporal evolutions of 2D signals. Our results show that the proposed QLE approach is capable of describing vibrational relaxation, decoherence, and vibrational coherence transfer, as well as their manifestations in spectroscopic signals. Furthermore, vibrational quantum beats specific for excited-state vs ground-state nuclear wave packet dynamics can also be identified. We anticipate that this method will provide a useful tool to conduct theoretical studies of 2D spectroscopy for strong vibronically coupled systems and to elucidate intricate vibronic couplings in complex molecular systems.

I. INTRODUCTION

Two-dimensional electronic spectroscopy (2DES) has become an important experimental technique to study ultrafast electronic and molecular dynamics in a broad range of molecular systems,[1–10] such as molecular aggregates,[11,12] semiconductors,[13] photochemical reactions,[14] and photosynthetic light-harvesting complexes.[4,15–17] As a powerful tool for the elucidation of electronic couplings and solvation dynamics in the condensed phase, experimental 2DES spectra provide abundant information on molecular dynamics and interactions between a molecular system and its surroundings.[3,17,18] However, the congested spectroscopic signals and the complex spectral and temporal dynamics often limit the quantitative interpretation of experimental observations. Therefore, the development of theoretical simulations of 2DES spectra is necessary for the analysis of experimental results and the elucidations of dynamical processes in the condensed phase.

Recent advances in vibrationally resolved 2D spectroscopic techniques have enabled direct probing of intricate couplings between vibrational and electronic degrees of freedom, which plays a crucial role in photophysical properties of molecular systems.[7,12,19–22] For example, the two-dimensional electronic-vibrational (2DEV) spectroscopy developed by Oliver *et al.* has provided a new experimental approach to resolve the dynamics on both electronic and vibrational degrees of freedom and to assess the vibronic couplings of molecular systems.[23] Nevertheless, the inclusion of vibrational degrees of freedom complicates the theoretical descriptions of 2DES spectroscopy, and the relevant simulations of 2D spectra with explicit treatment of vibrational dynamics, such as vibrational coherences and vibrational relaxations, are underdeveloped.[24–26] Hence, an efficient way to simulate the 2D spectra in a condensed-phase environment with both electronic and vibrational degrees of freedom treated explicitly has great importance in providing insight into the experimental manifestations of intricate vibronic couplings and environmental effects.

The standard theoretical description of nonlinear spectroscopy is based on the response function formalism.[27] Specifically, four-wave mixing experiments such as 2DES are described by the third-order polarization. Under the impulsive limit, the third-order polarization can be calculated by the impulsive response function analytically for simple model systems such as Brownian harmonic oscillators. For complicated systems with nontrivial system–bath interactions, additional approximations have to be invoked and numerical evaluations of impulsive response functions can be carried out by incorporating dynamical theories, i.e., the hierarchical equations of motion (HEOM) method,[28–30] to describe the time-evolution of the system after field–matter interactions. To simulate 2DES spectra, the response-function based methods have the advantage of simple extraction of the signals at the phase-matching direction, readily achieved by selective calculations of particular terms in the response functions that satisfy the given phase-matching condition. However, when the dimensionality of the system is large, the number of terms involved in the calculation grows dramatically. In addition, the impulsive response functions are unable to describe the pulse-overlap effects that have been shown experimentally[31] and theoretically[32] to exhibit nontrivial contributions to the features of 2DES spectra. Although the convolution between the pulse envelopes and the calculated response functions can be achieved by numerical integrations, the computational cost may become an issue.

The overlap of finite-width pulses can be naturally included by the dynamical simulation of 2DES spectra that explicitly propagate the system dynamics driven by three external fields, where the system is usually described by a reduced density matrix. However, this non-perturbative approach results in the total polarization that contains signals at all possible phase-matching directions. Hitherto, several schemes for the extraction of 2DES signals from dynamical simulations have been proposed and utilized in the simulations of condensed-phase 2DES spectra by the combination with dynamical theories.[32–43] Although the density-matrix based methods for 2DES simulations have been further developed in the past few decades, the method that emphasizes on the explicit treatment of vibrational relaxation dynamics is still underdeveloped. Furthermore, the computational cost of the density-matrix based method becomes formidable when applied to a multi-dimensional system, especially so when multiple vibrational states have to be considered. Therefore, the development of wavefunction based methods may provide an alternative approach to the simulations of 2DES spectra for multi-dimensional systems. Recently, several wavefunction approaches have been proposed for 2DES spectra simulations, including the methods based on propagating vibronic wavefunctions[44] or stochastic wavefunction approaches,[45,46] yet, so far, methods that focus on nuclear wave packet dynamics and vibrational relaxation are rather limited.

In this regard, we aim to develop a theoretical method that incorporates the influences of external laser fields into the explicit propagation of quantum dissipative wave packet dynamics, which enables efficient 2DES simulations for a multi-dimensional system with both pulse-overlap and environmental effects naturally included in a consistent framework. To this end, we proposed a non-perturbative method that combines multi-dimensional quantum Langevin equation (QLE) approach into the propagation of system dynamics with exact system–field interactions to perform dynamical simulations of 2DES spectra in the condensed phase. The QLE approach emphasizes the explicit treatment of vibrational excitations and their relaxation dynamics, enabling detailed descriptions of coupled electronic–nuclear dynamics. The structure of this paper is organized as follows: In Sec. II, we present our QLE approach by a generalization of the friction operator approach proposed by Messina and co-workers.[47,48] In addition, we outline a perturbative procedure to calculate the third-order polarization at the three-pulse photon-echo (3PPE) phase-matching direction by utilizing auxiliary wavefunctions propagated by a set of non-Hermitian Schrödinger equations and provide the computational details of numerical simulations. In Sec. III, we applied the QLE approach to a displaced-oscillator model to demonstrate its capability to simulate the 2DES spectra in a dissipative environment. The spectral and temporal evolutions of spectroscopic signals in the simulated rephasing and non-rephasing spectra under the influences of a dissipative environment are discussed, and the results indicate that the QLE approach can describe the vibrational relaxation, coherence transfer, and vibrational decoherence manifested by the dissipative wave packet dynamics. In Sec. IV, we summarize the main results and discuss the general applicability of our method.

II. METHODS

A. Quantum Langevin equation

To describe the wave packet dynamics in a dissipative condensed-phase environment, we adopt a QLE to describe the effects of a dissipative environment (bath) on wave packet dynamics. Considering an open quantum system described by a general system–bath model, the corresponding equations of motion in the Heisenberg picture lead to the QLE that describes the effects of the environment in a friction kernel and random force that arise from thermalized bath motions.[49,50] To implement QLE in quantum dynamical simulations, one can incorporate the friction and random force terms into a friction operator $F(t)$ and simulate dissipative wave packet dynamics by propagating a modified time-dependent Schrödinger equation (TDSE),[47]

$$i\hbar\frac{\partial}{\partial t}|\Psi(\boldsymbol{r},t)\rangle = [H + F(t)]|\Psi(\boldsymbol{r},t)\rangle. \tag{1}$$

This approach has been applied to describe systems with two electronic states and one vibrational mode.[48] In this paper, we generalize the approach in Ref. 48 to treat multi-dimensional systems, which enable simulations of dissipative quantum dynamics in general molecular systems.

We consider a system with N electronic states and M vibrational modes. The total wavefunction Ψ can be written as

$$|\Psi(\boldsymbol{r},t)\rangle = \sum_{n=1}^{N}\psi_n(\boldsymbol{r},t)|n\rangle, \tag{2}$$

where $|n\rangle$ denotes the nth electronic state and $\psi_n(r,\ t)$ is a M-dimensional time-dependent nuclear wavefunction associated with

$|n\rangle$. The total wavefunction satisfies the normalization condition,

$$\langle \Psi(\boldsymbol{r},t)|\Psi(\boldsymbol{r},t)\rangle = 1, \tag{3}$$

which leads to

$$\sum_{n=1}^{N}\int |\psi_n(\boldsymbol{r},t)|^2 d\boldsymbol{r} = 1. \tag{4}$$

For the N-state M-mode system, the Hamiltonian can be written as

$$\begin{aligned} H = &\sum_n\left[-\frac{\hbar^2}{2}\sum_{i=1}^{M}\frac{1}{m_i}\frac{\partial^2}{\partial r_i^2} + V_n(\boldsymbol{r})\right]|n\rangle\langle n| \\ &+\sum_n\sum_{m\neq n} J_{nm}(\boldsymbol{r})|n\rangle\langle m|, \end{aligned} \tag{5}$$

where m_i is the effective mass of the ith vibrational mode, $V_n(\boldsymbol{r})$ is the potential of the nth electronic state, and $J_{nm}(\boldsymbol{r})$ is the interstate coupling between $|n\rangle$ and $|m\rangle$. Note that we formulate the Hamiltonian in a quasi-diabatic basis of the electronic states such that the interstate couplings are non-zero and the derivative coupling terms can be effectively neglected. Furthermore, we substitute Eq. (2) into TDSE and project onto $|n\rangle$ to obtain

$$\begin{aligned} i\hbar\frac{\partial}{\partial t}\psi_n(\boldsymbol{r},t) = &\left[-\frac{\hbar^2}{2}\sum_{i=1}^{M}\frac{1}{m_i}\frac{\partial^2}{\partial r_i^2} + V_n(\boldsymbol{r})\right]\psi_n(\boldsymbol{r},t) \\ &+\sum_{m\neq n} J_{nm}(\boldsymbol{r})\psi_m(\boldsymbol{r},t). \end{aligned} \tag{6}$$

To derive a QLE, we consider the following time-dependent expectation values:

$$\langle r_i\rangle_n(t) = \frac{\int \psi_n^*(\boldsymbol{r},t) r_i \psi_n(\boldsymbol{r},t) d\boldsymbol{r}}{\int |\psi_n(\boldsymbol{r},t)|^2 d\boldsymbol{r}}, \tag{7}$$

$$\langle p_i\rangle_n(t) = \frac{\int \psi_n^*(\boldsymbol{r},t) p_i \psi_n(\boldsymbol{r},t) d\boldsymbol{r}}{\int |\psi_n(\boldsymbol{r},t)|^2 d\boldsymbol{r}}, \tag{8}$$

where r_i and p_i are the position and momentum operators of the ith vibrational mode, respectively. Here, we use the angle bracket $\langle\cdot\rangle_n$ to denote the average over the vibrational wave packet at the nth electronic state, and the vibrational wavefunction associated with each electronic state is independently renormalized to obtain the expectation values. From Eq. (6), one would expect that the equations of motion for $\langle r_i\rangle_n(t)$ and $\langle p_i\rangle_n(t)$ should depend on the vibrational wave packet at different electronic states,

$$\begin{aligned} \frac{\partial}{\partial t}\langle r_i\rangle_n(t) &= \frac{\partial}{\partial t}(\langle\psi_n|r_i|\psi_n\rangle)\Big/\int |\psi_n(\boldsymbol{r},t)|^2 d\boldsymbol{r} \\ &= \frac{1}{m_i}\langle p_i\rangle_n + \frac{i}{\hbar}\sum_{m\neq n}\left[\int \psi_m^*(\boldsymbol{r},t)J_{mn}(\boldsymbol{r}) r_i \psi_n(\boldsymbol{r},t) d\boldsymbol{r}\right. \\ &\quad \left. - \int \psi_n^*(\boldsymbol{r},t)J_{nm}(\boldsymbol{r}) r_i \psi_m(\boldsymbol{r},t) d\boldsymbol{r}\right]\Big/\int |\psi_n(\boldsymbol{r},t)|^2 d\boldsymbol{r}, \end{aligned} \tag{9}$$

$$\begin{aligned} \frac{\partial}{\partial t}\langle p_i\rangle_n(t) &= \frac{\partial}{\partial t}(\langle\psi_n|p_i|\psi_n\rangle)\Big/\int |\psi_n(\boldsymbol{r},t)|^2 d\boldsymbol{r} \\ &= -\left\langle\frac{\partial V_n}{\partial r_i}\right\rangle_n + \frac{i}{\hbar}\sum_{m\neq n}\left[\int \psi_m^*(\boldsymbol{r},t)J_{mn}(\boldsymbol{r}) p_i \psi_n(\boldsymbol{r},t) d\boldsymbol{r}\right. \\ &\quad \left. - \int \psi_n^*(\boldsymbol{r},t)J_{nm}(\boldsymbol{r}) p_i \psi_m(\boldsymbol{r},t) d\boldsymbol{r}\right]\Big/\int |\psi_n(\boldsymbol{r},t)|^2 d\boldsymbol{r}, \end{aligned} \tag{10}$$

where dividing by $\int|\psi_n(\boldsymbol{r},t)|^2 d\boldsymbol{r}$ represents the intermediated renormalization of the expectation values, and therefore, the time derivative of this term is not considered. In addition, integrals involving interstate coupling $J_{nm}(r)$ depend on the overlap between wave packets on different electronic potential energy surfaces (ψ_n and ψ_m). In the limit of zero electronic coupling or when one of the wave packets is far away from the strong electronically coupled regime on the nuclear coordinates, these interstate coupling terms can be safely ignored. Generally speaking, in a condensed-phase environment, the rapid dephasing between the wave packets at different states should lead to small contributions from these interstate coupling terms such that the time evolutions of vibrational wave packets on different electronic states are independent of each other. Therefore, we assume that ψ_n and ψ_m are strongly dephased and their correlations are negligible, and as a result, interstate coupling terms in Eqs. (9) and (10) can be ignored. In addition, we expand the potential $V_n(\boldsymbol{r})$ with respect to $\langle\boldsymbol{r}\rangle_n(t)$ up to second-order in the displacements,

$$\begin{aligned} V_n(\boldsymbol{r}) \approx &\sum_{i=1}^{M} V_n(\langle r_i\rangle_n(t)) + \sum_{i=1}^{M}\left(\frac{\partial V_n}{\partial r_i}\right)_{r_i=\langle r_i\rangle_n(t)}(r_i - \langle r_i\rangle_n(t)) \\ &+\frac{1}{2}\sum_{i=1}^{M}\sum_{j=1}^{M}\left(\frac{\partial^2 V_n}{\partial r_i \partial r_j}\right)_{r_i=\langle r_i\rangle_n(t), r_j=\langle r_j\rangle_n(t)} \\ &\times(r_i - \langle r_i\rangle_n(t))(r_j - \langle r_j\rangle_n(t)). \end{aligned} \tag{11}$$

Therefore, the equations of motion for $\langle r_i\rangle_n(t)$ and $\langle p_i\rangle_n(t)$ can be simplified to obtain

$$\frac{\partial}{\partial t}\langle r_i\rangle_n(t) = \frac{1}{m_i}\langle p_i\rangle_n(t), \tag{12}$$

$$\frac{\partial}{\partial t}\langle p_i\rangle_n(t) = -\left(\frac{\partial V_n}{\partial r_i}\right)_{r_i=\langle r_i\rangle_n(t)}. \tag{13}$$

Note that these equations of motion are consistent with the Ehrenfest theorem for each individual potential energy surface, not the full averaged potential. Provided that a system can be characterized by a set of smooth potential energy surfaces, the second-order expansion of potential with respect to the center of the wave packet yields good approximations of the dynamics near the potential energy minima.[51]

To incorporate the effects of the environment, we modify the equations of motion by recasting Eq. (13) into the form of a QLE,[49,50]

$$\begin{aligned} \frac{\partial}{\partial t}\langle p_i\rangle_n(t) = &-\left(\frac{\partial V_n}{\partial r_i}\right)_{r_i=\langle r_i\rangle_n(t)} - \frac{2}{m_i}\int_0^t \eta_{n,i}(t-t')\langle p_i\rangle_n(t')dt' \\ &-2\eta_{n,i}(t)\langle r_i\rangle_n(0) + f_{n,i}(t), \end{aligned} \tag{14}$$

where $\eta_{n,i}(t)$ and $f_{n,i}(t)$ are the friction kernel and random force of the ith vibrational mode on the nth electronic state, respectively.

Equation (14) allows us to relate time derivatives of $\langle p_i \rangle_n(t)$ to frictional interactions. Consequently, we follow Ref. 47 to construct a friction operator that is consistent with the QLE. To this end, we apply the Gaussian wave packet approximation (GWA) by assuming that the vibrational wave packet associated with the nth electronic state can be represented by a M-dimensional Gaussian function,[51,52]

$$\begin{aligned}\psi_n(\boldsymbol{r},t) = C\exp\Bigg\{\frac{i}{\hbar}\sum_{i=1}^{M}\Big[\alpha_{n,ii}(t)(r_i - \langle r_i\rangle_n(t))^2 \\ + \sum_{j\neq i}\beta_{n,ij}(t)(r_i - \langle r_i\rangle_n(t))(r_j - \langle r_j\rangle_n(t)) \\ + \langle p_i\rangle_n(r_i - \langle r_i\rangle_n(t)) + \gamma_n(t)\Big]\Bigg\},\end{aligned} \tag{15}$$

where C is an constant amplitude, $\langle \boldsymbol{r}\rangle_n(t)$ corresponds to the center of the wave packet on the nth electronic state, the time-dependent parameters $\alpha_{n,i}(t)$, $\beta_{n,ij}(t)$ are related to the spread of the wave packet, and $\gamma_n(t)$ is a time-dependent phase. Note that for a Gaussian wave packet, the evolution of time-dependent parameters can be determined by taking the time derivative of $\psi_n(\boldsymbol{r}, t)$ in Eq. (15) and evaluating the derivatives according to the chain rule. By comparing $\frac{\partial}{\partial t}\psi_n(\boldsymbol{r},t)$ calculated from Eq. (15) with the modified Schrödinger equation [Eq. (1)], one finds that additional terms related to the environmental effects can be collected in a term linear in $(r_i - \langle r_i\rangle_n(t))$,[47] which allows us to define the friction operator of the nth electronic state $F_n(t)$ as

$$\begin{aligned}F_n(t) = \sum_{i=1}^{M}\Bigg[\frac{2}{m_i}\int_0^t \eta_{n,i}(t-t')\langle p_i\rangle_n(t')dt' + m_i\eta_{n,i}(t)\langle r_i\rangle_n(0) \\ - f_{n,i}(t)\Bigg]\big[r_i - \langle r_i\rangle_n(t)\big]|n\rangle\langle n|.\end{aligned} \tag{16}$$

Note that the friction operator is diagonal in the electronic basis, which is a consequence of neglecting the off-diagonal terms in Eqs. (9) and (10) and is consistent with diagonal system–bath interacting models commonly adopted in describing open quantum system dynamics. On the other hand, $F_n(t)$ is linear in $(r_i - \langle r_i\rangle_n(t))$, which could induce transitions between vibrational states. Therefore, vibrational relaxation dynamics could be reasonably described by the QLE. Finally, for simplicity, we consider the Markovian limit in this work and replace the friction kernel $\eta_{n,i}(t)$ by $\eta_{n,i}\delta(t)$, where $\eta_{n,i}$ becomes a constant friction coefficient. In this limit, the friction operator [Eq. (16)] can be simplified as

$$F_n(t) = \sum_{i=1}^{M}\Bigg[\frac{\eta_{n,i}}{m_i}\langle p_i\rangle_n(t) - f_{n,i}(t)\Bigg]\big[r_i - \langle r_i\rangle_n(t)\big]|n\rangle\langle n|. \tag{17}$$

We further assume that the random forces satisfy the fluctuation–dissipation relation,

$$\langle f_{n,i}(t)f_{n,j}(t')\rangle = 2\eta_{n,i}k_BT\delta(t-t')\delta_{i,j}. \tag{18}$$

According to the form of $F_n(t)$, the friction operator can be interpreted as the negative work done by the net force exerted by the environment. Moreover, $F_n(t)$ is determined by the expectation value of the position $\langle r_i\rangle_n$ and the momentum $\langle p_i\rangle_n$ of the vibrational wave packet. Upon averaging, $\langle[\rho^{eq}, F_n(t)]\rangle = 0$, where ρ^{eq} is the equilibrium density matrix, and thus, the equilibrium should be maintained. Therefore, the method proposed in this work should maintain a thermal equilibrium distribution. However, whether or not the QLE approach strictly satisfies the detailed balance is a nontrivial problem that requires further investigation in the future. With the friction operator for each electronic state, the dissipative wave packet dynamics can be simulated by propagating TDSE with the modified total Hamiltonian,

$$i\hbar\frac{\partial}{\partial t}|\Psi(\boldsymbol{r},t)\rangle = \Bigg[H + \sum_{n=1}^{N}F_n(t)\Bigg]|\Psi(\boldsymbol{r},t)\rangle. \tag{19}$$

Equations (17) and (19) can be used to propagate the total wavefunction $\Psi(\boldsymbol{r}, t)$ under the influence of a frictional bath given the friction coefficient and the random force drawn from a temperature-dependent Gaussian random variable in accordance with Eq. (18). Equation (19) represents a Schrödinger–Langevin equation that contains two forces describing the environmental effects on the system dynamics: the frictional force $[\frac{\eta_{n,i}}{m_i}\langle p_i\rangle_n(t)]$ and the random force $[f_{n,i}(t)]$.[53,54] While the random force term describes thermal fluctuations induced by bath equilibrium dynamics, the frictional force term represents a mean dissipative field created by averaging over the bath influences. The dynamical equation specifically separates dissipation from fluctuations and should be considered as a feature of the Schrödinger–Langevin approach. Note that while random fluctuation terms also emerge from a stochastic Schrödinger equation (SSE) formulation of open quantum system dynamics, the stochastic terms in the SSE approach do not distinguish dissipation from fluctuation and therefore should not be directly compared to the random force term in the QLE approach.[55] Moreover, since we formulate the Hamiltonian in a quasi-diabatic basis, the unmodified Hamiltonian H could have scalar electronic couplings that lead to electronic transitions, and the friction operator amounts to effects due to diagonal random noise linear in the displacements. As a result, both electronic transitions and vibrational relaxations are described in this QLE approach.

In summary, we derived the friction operator for a QLE approach for dissipative wave packet dynamics in a multistate–multimode system based on the following assumptions. We formulate the problem in a quasi-diabatic electronic basis to avoid the derivative coupling terms and further assume that the correlations between vibrational wave packets at different electronic states are negligible, which is justified if the wave packets at different electronic states are strongly dephased such that the dynamics of each wave packet is nearly independent and occurs on a single potential energy surface. In addition, the GWA is applied so that we can use a simple Gaussian *Ansatz* to derive the friction operator, which is a good approximation for nuclear motions near the vicinity of the potential energy minima. The derived friction operator provides an explicit treatment of vibrational relaxation dynamics within an electronic state and could be connected to the influences induced by a microscopic bath model.[53,55,56] Nevertheless, the electronic decoherence induced by a dissipative environment is not explicitly described by the friction operator presented in this work. Various explicit treatments of electronic decoherence in wave packet dynamics by incorporating a stochastic bath derived from microscopic system–bath interactions have been reported previously (see Refs. 57 and 58). These stochastic bath methods mostly focus on the electronic dynamics and do not properly treat vibrational relaxations. Therefore, we emphasize the QLE approach for dissipative wave packet dynamics in this work and do not intend to treat electronic decoherence. Nonetheless, the QLE approach presented here can be implemented together with a stochastic bath method for electronic decoherence in dynamical or spectroscopic simulations to complement the part of dissipative nuclear dynamics. Note that we have only assumed that the potential of the system is a smooth function throughout the derivation, and thus, the presented approach for implementing QLE is not restricted to harmonic systems. Moreover, the functional form of the friction operator is simple and is readily implemented numerically. Thus, our generalized multi-dimensional QLE approach can provide a simple scheme for dissipative quantum wave packet dynamics simulations of common molecular systems.

B. Photon-echo polarization

The theoretical description of 2DES is related to the third-order polarization at a specific phase-matching direction. For the dynamical simulation of signals in such a four-wave mixing experiment, we directly simulate the system interaction with three external laser pulses,

$$i\hbar\frac{\partial}{\partial t}|\Psi(t)\rangle = [H_0 + H_{int}(t)]|\Psi(t)\rangle, \tag{20}$$

where the system is described by a time-independent zeroth-order Hamiltonian H_0 and the field–matter interaction Hamiltonian $H_{int}(t)$ is represented by the molecular dipole Hamiltonian,

$$\begin{aligned} H_{int}(t) &= -\mu\cdot\sum_{a=1}^{3}\boldsymbol{E}_a(t), \\ &= -\mu\sum_{a=1}^{3}\Lambda_a(t,\tau_a)\Big(e^{i\boldsymbol{k}_a\cdot\boldsymbol{r}-i\omega_a(t-\tau_a)} + c.c.\Big). \end{aligned} \tag{21}$$

Here, the dipole operator is denoted as μ and the electric field of the ath laser pulse $\boldsymbol{E}_a(t)$ is described by its envelope $\Lambda_a(t, \tau_a)$, wave vector $\boldsymbol{k}_a$, central frequency ω_a, and pulse central time τ_a. With the interaction Hamiltonian, we can define the third-order polarization through the time-dependent perturbation theory (TDPT). According to TDPT, we treat the field–matter interaction as a perturbation to the system, and the corresponding nth-order wavefunction is defined as

$$\begin{aligned} \left|\phi^{(n)}(t)\right\rangle = \left(-\frac{i}{\hbar}\right)^n \int_0^t d\tau_n \int_0^{\tau_n} d\tau_{n-1}\cdots\int_0^{\tau_2} d\tau_1 U_0(t) \\ \times H_{int,I}(\tau_n)H_{int,I}(\tau_{n-1})\cdots H_{int,I}(\tau_1)|\phi(0)\rangle. \end{aligned} \tag{22}$$

Here, $U_0(t)$ denotes the time-evolution operator defined by H_0, and the subscript I represents the operator in the interaction picture, $H_{int,I}(t) = U_0^\dagger(t)H_{int}(t)U_0(t)$. By definition, the total polarization is defined as the expectation value of the dipole operator μ, and the corresponding Nth-order polarization $P^{(N)}(t)$ can be calculated by

$$P^{(N)}(t) = \sum_{m=0}^{N}\left\langle\phi^{(N-m)}(t)|\mu|\phi^{(m)}(t)\right\rangle, \tag{23}$$

where the sum of the order of ket and bra equals to N for each term in $P^{(N)}(t)$. In particular, we consider the case of $N = 3$,

$$P^{(3)}(t) = \sum_{m=0}^{3}\left\langle\phi^{(3-m)}(t)|\mu|\phi^{(m)}(t)\right\rangle. \tag{24}$$

Note that in $H_{int}(t)$, each laser field contains both $+\boldsymbol{k}$- and $-\boldsymbol{k}$-components, and as a result, the polarization calculated by Eq. (24) includes signals at all possible phase-matching directions (i.e., $\boldsymbol{k}_s = \pm\boldsymbol{k}_1 \pm\boldsymbol{k}_2 \pm\boldsymbol{k}_3$).

For density-matrix based dynamical simulations, both perturbative and non-perturbative approaches have been proposed to calculate the photon-echo signals. To extract the third-order polarization at a phase-matching direction corresponding to the 2DES experiment, it can be done non-perturbatively by the linear combination of the total polarizations calculated at different phase angles.[33–36] Although the idea of this phase-cycling approach is straightforward, the computational cost is too high to be useful in calculating the 2DES signals of a general multi-dimensional system. Alternatively, the equation-of-motion phase-matching-approach (EOM-PMA) proposed by Domcke and co-workers[37,38] has provided an efficient method to obtain the third-order polarization at a given phase-matching direction through a perturbative procedure. The EOM-PMA method has been incorporated into various dynamical theories and applied to simulate the effects of a dissipative environment on 2DES spectra, such as Redfield theory,[37,38] time-nonlocal quantum master equation,[39–41] and HEOM.[32,42,43,59] However, the computational efficiency of the density-matrix based method decreases with the increase in the dimensionality of the molecular system. Numerically, for a system described by N basis states, the computational cost of density-matrix based methods scales as $\mathcal{O}(N^2)$, whereas the wavefunction based methods scale as $\mathcal{O}(M\times N)$ for M trajectories, which can be individually calculated by parallel computing. Therefore, the wavefunction based method may provide a more efficient way for 2DES spectra simulations of a general molecular system with the consideration of both equally important electronic and vibrational degrees of freedom.

To extract the third-order polarization at a particular phase-matching direction through wavefunction based quantum dynamical simulations, we first adjust the form of $H_{int}(t)$ so that the phase-matching condition can be achieved. We rewrite the dipole operator into the corresponding excitation part X and de-excitation part $X^\dagger$,

$$\begin{aligned} \mu &= \sum_n \sum_{\{n'|\epsilon_{n'}>\epsilon_n\}} \mu_{nn'}|n\rangle\langle n'| + \mu_{n'n}|n'\rangle\langle n| \\ &\equiv X + X^\dagger, \end{aligned} \tag{25}$$

where $\mu_{n,n'}$ denotes the transition dipole moment between states n and n' with energy $\epsilon_n \leq \epsilon_{n'}$. Using the fact that the photo-induced excitation and de-excitation (or emission) are associated with the direction of the wave vector [that is, given small laser detuning, the excitation (de-excitation) of ket (bra) is dominated by the contribution from the $+\boldsymbol{k}$-component of the laser field, and vice versa], we recast $H_{int}(t)$ into the following form:

$$\begin{aligned} H_{int}(t) &= -X\sum_{a=1}^{3}\Lambda_a(t,\tau_a)e^{-i\omega_a(t-\tau_a)} + h.c. \\ &\equiv -\sum_{a=1}^{3}\Big(V_a(t) + V_a^\dagger(t)\Big). \end{aligned} \tag{26}$$

As the effect of $e^{i\boldsymbol{k}\cdot\boldsymbol{r}}\big(e^{-i\boldsymbol{k}\cdot\boldsymbol{r}}\big)$ is embedded in the operator $X\big(X^\dagger\big)$, a specific phase-matching condition can be realized by selective combinations of $V_a(t)$ and $V_a^\dagger(t)$ in $H_{int}(t)$. For the simulation of 2DES signals, we consider the 3PPE polarization with the phase-matching direction $\boldsymbol{k}_s = -\boldsymbol{k}_1 + \boldsymbol{k}_2 + \boldsymbol{k}_3$, and the corresponding interaction Hamiltonian becomes

$$H_{int}(t) = -V_1(t) - V_2^\dagger(t) - V_3^\dagger(t). \tag{27}$$

Note that the 3PPE polarization corresponds to the system interaction with each pulse in first order, that is, each of the $H_{int,I}(t)$ in Eq. (22) corresponds to one of $V_1(t)$, $V_2^\dagger(t)$, and $V_3^\dagger(t)$. Given that the initial state is the electronic ground state, which cannot be annihilated ($X|g\rangle = \langle g|X^\dagger = 0$) and that the time-ordering of each pulse can be interchanged, we obtain the 3PPE polarization, which corresponds to the nonzero terms in Eq. (24),

$$\begin{aligned} P_{PE}^{(3)}(t) =& \left\langle \phi_{101^\dagger}^{(2)}(t)|X|\phi_{01^\dagger 0}^{(1)}(t)\right\rangle + \left\langle \phi_{11^\dagger 0}^{(2)}(t)|X|\phi_{001^\dagger}^{(1)}(t)\right\rangle \\ &+ \left\langle \phi_{100}^{(1)}(t)|X|\phi_{01^\dagger 1^\dagger}^{(2)}(t)\right\rangle + \left\langle \phi_{000}^{(0)}(t)|X|\phi_{11^\dagger 1^\dagger}^{(3)}(t)\right\rangle. \end{aligned} \tag{28}$$

Here, $\left|\phi_{a^{(\dagger)}b^{(\dagger)}c^{(\dagger)}}^{(n)}(t)\right\rangle$, where a, b, and c are integers of either 0 or 1 and $n = a + b + c$ denotes a nth-order contribution caused by interacting with laser pulses 1, 2, and 3 by a number of a, b, and c times, respectively. For instance, $\left|\phi_{01^\dagger 1^\dagger}^{(2)}(t)\right\rangle$ represents the second-order contribution due to the interaction with the second pulse and third pulse once each and no interaction with the first pulse. The other terms in Eq. (28) can be understood in a similar fashion. Terms in Eq. (28) include the Liouville pathways of ground state bleaching (GSB), stimulated emission (SE), and excited state absorption (ESA). Note that the bras and kets in Eq. (28) do not represent physical states; the Dirac notation used in Eq. (28) is merely a notation of vectors for simplicity. Furthermore, these perturbative terms cannot be obtained by solving the TDSE directly. If we propagate a wavefunction by a specific combination of field–matter interactions as

$$\begin{aligned} i\hbar\frac{\partial}{\partial t}|\psi_{a^{(\dagger)}b^{(\dagger)}c^{(\dagger)}}(t)\rangle =& \left[H_0 - aV_1^{(\dagger)}(t) - bV_2^{(\dagger)}(t) - cV_3^{(\dagger)}(t)\right] \\ &\times |\psi_{a^{(\dagger)}b^{(\dagger)}c^{(\dagger)}}(t)\rangle, \end{aligned} \tag{29}$$

then the auxiliary wavefunction $|\psi_{a^{(\dagger)}b^{(\dagger)}c^{(\dagger)}}(t)\rangle$ would contain all orders of perturbative contributions due to combinations of the three field–matter interactions because the wavefunction evolved by Eq. (29) can interact with each pulse an arbitrary number of times. Thus, $\left|\phi_{a^{(\dagger)}b^{(\dagger)}c^{(\dagger)}}^{(n)}(t)\right\rangle \neq |\psi_{a^{(\dagger)}b^{(\dagger)}c^{(\dagger)}}(t)\rangle$. In order to extract the $\left|\phi_{a^{(\dagger)}b^{(\dagger)}c^{(\dagger)}}^{(n)}(t)\right\rangle$ terms used in Eq. (28), we treat the wavefunction defined by Eq. (29) as an auxiliary wavefunction, which acts as a mathematical tool to the desired perturbative contributions. In the weak-field limit, we can derive the formula for the calculation of 3PPE polarization by a perturbative scheme. The derivation is presented in the Appendix, and the formulas that relate terms in Eq. (28) to auxiliary wavefunctions defined by Eq. (29) are given by Eqs. (A10)–(A16). The presented method for calculating third-order polarization at a particular phase-matching direction is in the same spirit as the EOM-PMA proposed by Krčmář *et al.*[44] In addition, the procedure described in this section can also be applied to the calculations of other four-wave mixing signals and be generalized to other nonlinear responses.

C. Simulation of 2DES spectra

To simulate the 2DES signals in a condensed-phase environment, we incorporate the QLE approach (Sec. II A) with the simulation of quantum wave packet dynamics under the influences of external fields. For a system with N electronic states described by a time-independent Hamiltonian H_s, the 3PPE polarization can be calculated by the auxiliary wavefunctions [Eqs. (28) and (A10)–(A16)] propagated by the following auxiliary Schrödinger equations:

$$\begin{aligned} i\hbar\frac{\partial}{\partial t}&|\psi_{11^\dagger 1^\dagger}(t)\rangle \\ &= \left[H_s + F(t) - V_1(t) - V_2^\dagger(t) - V_3^\dagger(t)\right]|\psi_{11^\dagger 1^\dagger}(t)\rangle, \end{aligned} \tag{30}$$

$$i\hbar\frac{\partial}{\partial t}|\psi_{11^\dagger 0}(t)\rangle = \left[H_s + F(t) - V_1(t) - V_2^\dagger(t)\right]|\psi_{11^\dagger 0}(t)\rangle, \tag{31}$$

$$i\hbar\frac{\partial}{\partial t}|\psi_{1^\dagger 10}(t)\rangle = \left[H_s^\dagger + F^\dagger(t) - V_1^\dagger(t) - V_2(t)\right]|\psi_{1^\dagger 10}(t)\rangle, \tag{32}$$

$$i\hbar\frac{\partial}{\partial t}|\psi_{101^\dagger}(t)\rangle = \left[H_s + F(t) - V_1(t) - V_3^\dagger(t)\right]|\psi_{101^\dagger}(t)\rangle, \tag{33}$$

$$i\hbar\frac{\partial}{\partial t}|\psi_{1^\dagger 01}(t)\rangle = \left[H_s^\dagger + F^\dagger(t) - V_1^\dagger(t) - V_3(t)\right]|\psi_{1^\dagger 01}(t)\rangle, \tag{34}$$

$$i\hbar\frac{\partial}{\partial t}|\psi_{01^\dagger 1^\dagger}(t)\rangle = \left[H_s + F(t) - V_2^\dagger(t) - V_3^\dagger(t)\right]|\psi_{01^\dagger 1^\dagger}(t)\rangle, \tag{35}$$

$$i\hbar\frac{\partial}{\partial t}|\psi_{1^\dagger 00}(t)\rangle = \left[H_s^\dagger + F^\dagger(t) - V_1^\dagger(t)\right]|\psi_{1^\dagger 00}(t)\rangle. \tag{36}$$

$$i\hbar\frac{\partial}{\partial t}|\psi_{01^\dagger 0}(t)\rangle = \left[H_s + F(t) - V_2^\dagger(t)\right]|\psi_{01^\dagger 0}(t)\rangle, \tag{37}$$

$$i\hbar\frac{\partial}{\partial t}|\psi_{001^\dagger}(t)\rangle = \left[H_s + F(t) - V_3^\dagger(t)\right]|\psi_{001^\dagger}(t)\rangle, \tag{38}$$

$$i\hbar\frac{\partial}{\partial t}|\psi_{000}(t)\rangle = [H_s + F(t)]|\psi_{000}(t)\rangle. \tag{39}$$

Note that the total Hamiltonian is non-Hermitian due to the selective field–matter interactions such that the Schrödinger equation for bra and ket states has to be propagated separately. By definition, $\langle\psi_{abc}(t)| \equiv |\psi_{a^\dagger b^\dagger c^\dagger}(t)\rangle^\dagger$, and we can recast the Schrödinger equations for a bra into an equivalent ket Schrödinger equation.

In 2DES, the interactions between the system and three laser pulses are characterized by three delay times: coherence time τ, population time T, and detection time t. At a given population time, the corresponding 2DES spectrum is obtained by the 2D Fourier transform,

$$S(\omega_\tau, T, \omega_t) \sim \int_{-\infty}^{\infty} d\tau \int_0^{\infty} dt\, e^{-i\omega_\tau \tau} e^{i\omega_t t} \times iP_{PE}^{(3)}(\tau, T, t), \tag{40}$$

$$S_R(\omega_\tau, T, \omega_t) \sim \int_0^{\infty} d\tau \int_0^{\infty} dt\, e^{-i\omega_\tau \tau} e^{i\omega_t t} \times iP_{PE}^{(3)}(\tau, T, t), \tag{41}$$

$$S_{NR}(\omega_\tau, T, \omega_t) \sim \int_{-\infty}^{0} d\tau \int_0^{\infty} dt\, e^{-i\omega_\tau \tau} e^{i\omega_t t} \times iP_{PE}^{(3)}(\tau, T, t), \tag{42}$$

where the subscripts R and NR denote rephasing and non-rephasing spectra, respectively.

D. Basis-set expansion

For efficient numerical simulations, a matrix representation of operators can be obtained by choosing a set of basis functions. In general, for different electronic states, different sets of orthonormal functions can be used. In particular, considering a system with N electronic states and M vibrational modes, we can choose a set of basis functions for the nth electronic state that satisfies

$$\sum_{\alpha} |\phi_{n\alpha}\rangle\langle\phi_{n\alpha}| = I, \tag{43}$$

where the electronic state-specific basis functions $|\phi_{n\alpha}\rangle$ form a set of M-dimensional orthonormal functions. $|\phi_{n\alpha}\rangle$ could be further decomposed into a direct product of M basis functions for individual modes, but we chose to keep it general here. The total wavefunction can be represented by the linear combination of the basis functions,

$$\begin{aligned} |\Psi\rangle &= \sum_{n=1}^{N} |\psi_n\rangle \otimes |n\rangle \\ &= \sum_{n=1}^{N}\sum_{\alpha} c_{n\alpha}|\phi_{n\alpha}\rangle \otimes |n\rangle, \end{aligned} \tag{44}$$

where $c_{n\alpha} = \langle\phi_{n\alpha}|\psi_n\rangle$. The generic total Hamiltonian discussed in this study can be written as

$$\begin{aligned} H(t) &= H_s + F(t) + H_{int}(t) \\ &= \sum_{n=1}^{N}(\epsilon_n + h_n)|n\rangle\langle n| + \sum_{n=1}^{N}\sum_{n'\neq n} J_{nn'}|n\rangle\langle n'| \\ &\quad + \sum_{n=1}^{N} F_n(t) - \sum_{a=1}^{3} V_a^{(\dagger)}(t). \end{aligned} \tag{45}$$

Here, ϵ_n, h_n, and $J_{nn'}$ denote the electronic state energy, vibrational Hamiltonian, and the interstate coupling (in general, as a function of nuclear degrees of freedom), respectively. The corresponding matrix representation is

$$\begin{aligned} H_s &= \sum_{n=1}^{N}(\epsilon_n + h_n)|n\rangle\langle n| + \sum_{n=1}^{N}\sum_{n'\neq n} J_{nn'}|n\rangle\langle n'| \\ &= \sum_{n=1}^{N} \epsilon_n \cdot I \otimes |n\rangle\langle n| \\ &\quad + \sum_{n=1}^{N}\sum_{\alpha}\sum_{\alpha'} h_{n,\alpha\alpha'}|\phi_{n\alpha}\rangle\langle\phi_{n\alpha'}| \otimes |n\rangle\langle n| \\ &\quad + \sum_{n=1}^{N}\sum_{n'\neq n} J_{nn',\alpha\alpha'}|\phi_{n\alpha}\rangle\langle\phi_{n'\alpha'}| \otimes |n\rangle\langle n'|, \end{aligned} \tag{46}$$

$$\begin{aligned} F_n(t) &= \sum_{i=1}^{M}\left[\frac{\eta_{n,i}}{m_i}\langle p_i\rangle_n(t) - f_{n,i}(t)\right][r_i - \langle r_i\rangle_n(t)]|n\rangle\langle n| \\ &\equiv \sum_{i=1}^{M}\left(\Gamma_{n,i}(t) r_i - \tilde{\Gamma}_{n,i}(t)\right)|n\rangle\langle n| \\ &= \sum_{i=1}^{M}\sum_{\alpha}\sum_{\alpha'} \Gamma_{n,i}(t) r_{i,\alpha\alpha'}|\phi_{n\alpha}\rangle\langle\phi_{n\alpha'}| \otimes |n\rangle\langle n| \\ &\quad + \sum_{i=1}^{M} \tilde{\Gamma}_{n,i}(t) \cdot I \otimes |n\rangle\langle n|, \end{aligned} \tag{47}$$

$$\begin{aligned} V_a(t) &= X\Lambda_a(t,\tau_a)e^{-i\omega_a(t-\tau_a)} \\ &= \Lambda_a(t,\tau_a)e^{-i\omega_a(t-\tau_a)}\sum_{n=1}^{N}\sum_{\{n'|\epsilon_{n'}>\epsilon_n\}} \mu_{nn'}|n\rangle\langle n'| \\ &= \Lambda_a(t,\tau_a)e^{-i\omega_a(t-\tau_a)}\sum_{n=1}^{N}\sum_{\{n'|\epsilon_{n'}>\epsilon_n\}} \\ &\quad \times \sum_{\alpha}\sum_{\alpha'} \mu_{nn',\alpha\alpha'}|\phi_{n\alpha}\rangle\langle\phi_{n'\alpha'}| \otimes |n\rangle\langle n'|, \end{aligned} \tag{48}$$

where $\Gamma_{n,i}(t)$, $\tilde{\Gamma}_{n,i}(t)$, and the matrix elements are defined as

$$\Gamma_{n,i}(t) = \frac{\eta_{n,i}}{m_i}\langle p_i\rangle_n(t) - f_{n,i}(t), \tag{49}$$

$$\tilde{\Gamma}_{n,i}(t) = \Gamma_{n,i}(t)\cdot\langle r_i\rangle_n(t), \tag{50}$$

$$h_{n,\alpha\alpha'} = \langle\phi_{n\alpha}|h_n|\phi_{n\alpha'}\rangle, \tag{51}$$

$$J_{nn',\alpha\alpha'} = \langle\phi_{n\alpha}|J_{nn'}|\phi_{n'\alpha'}\rangle, \tag{52}$$

$$r_{i,\alpha\alpha'} = \langle\phi_{n\alpha}|r_i|\phi_{n\alpha'}\rangle, \tag{53}$$

$$\mu_{nn',\alpha\alpha'} = \langle\phi_{n\alpha}|\mu_{nn'}|\phi_{n'\alpha'}\rangle. \tag{54}$$

Note that in general, the transition dipole moment $\mu_{nn'}$ can be a function of nuclear coordinates. Under the Condon approximation, Eq. (54) becomes $\mu_{nn',\alpha\alpha'} = \mu_{nn'}\langle\phi_{n\alpha}|\phi_{n'\alpha'}\rangle$. Moreover, one can use a single set of basis functions for all electronic states, and the corresponding matrix representation is obtained by simply replacing $|\phi_{n\alpha}\rangle$ by $|\phi_{\alpha}\rangle$.

In reality, since the spectroscopic signals correspond to the transitions between the eigenstates of H_s, it is necessary to further transform the Hamiltonian into the eigenbasis representation. Assuming that H_s is Hermitian, we can define the unitary transformation matrix T, which consists of the eigenstates of H_s, and it can be obtained by the diagonalization of H_s,

$$\tilde{H}_s = T^{\dagger}H_sT. \tag{55}$$

With the transformation matrix T, we can transform the total wavefunction and the operators into the eigenbasis representation by

$$|\tilde{\Psi}\rangle = T^{\dagger}|\Psi\rangle, \tag{56}$$

$$\tilde{H}(t) = \tilde{H}_s + \tilde{F}(t) - \sum_{a=1}^{3}\tilde{V}_a^{(\dagger)}(t), \tag{57}$$

$$\tilde{F}(t) = T^{\dagger}F(t)T, \tag{58}$$

$$\tilde{V}_a(t) = T^{\dagger}V_a(t)T. \tag{59}$$

The 3PPE polarization can be calculated by numerical propagations of auxiliary Schrödinger equations in the eigenbasis representation. In this study, an iterative Crank–Nicolson scheme is adopted for the time propagations.

III. RESULTS AND DISCUSSIONS

A. Model system

To demonstrate the applicability of the QLE approach in 2DES simulations, we consider a model system described by two displaced 1D harmonic oscillators (in mass-weighted coordinates),

$$H_s = (\epsilon_g + h_g)|g\rangle\langle g| + (\epsilon_e + h_e)|e\rangle\langle e|, \tag{60}$$

$$h_g = \frac{1}{2}p^2 + \frac{1}{2}\omega_0^2 r^2, \tag{61}$$

$$h_e = \frac{1}{2}p^2 + \frac{1}{2}\omega_0^2 (r-d)^2. \tag{62}$$

Here, ϵ_g and ϵ_e are the electronic energies of ground and excited states, respectively. For the vibrational Hamiltonians h_g and h_e, ω_0 is the vibrational frequency and d corresponds to the difference between the equilibrium position of electronic ground and excited states. The parameters used in simulations carried out in this work are summarized in Table I. To describe the influences of a condensed-phase environment, we consider the Markovian friction and assume that the friction coefficients for different electronic states are the same. The corresponding friction operator is

$$\begin{aligned} F(t) &= F_g(t)|g\rangle\langle g| + F_e(t)|e\rangle\langle e| \\ &= \left(\Gamma_g(t)r - \tilde{\Gamma}_g(t)\right)|g\rangle\langle g| + \left(\Gamma_e(t)r - \tilde{\Gamma}_e(t)\right)|e\rangle\langle e|, \end{aligned} \tag{63}$$

$$\Gamma_n(t) = \eta\langle p\rangle_n(t) - f_n(t),\ (n = e, g), \tag{64}$$

$$\tilde{\Gamma}_n(t) = \Gamma_n(t)\cdot\langle r\rangle_n(t). \tag{65}$$

For the field–matter interactions, we consider the system interacting with Gaussian pulses,

$$\begin{aligned} V_a(t) &= X\cdot I_a e^{-4\ln 2\frac{(t-\tau_a)^2}{\tau_p^2}} e^{-i\omega_a(t-\tau_a)} \\ &= I_a e^{-4\ln 2\frac{(t-\tau_a)^2}{\tau_p^2}} e^{-i\omega_a(t-\tau_a)} \mu_{ge}|g\rangle\langle e|, \end{aligned} \tag{66}$$

where I_a is the intensity of the ath pulse and τ_p is the pulse width [full width at half maximum (FWHM)]. We further consider the Condon approximation such that μ_{ge} is a constant. In this study, the initial wave packet is set to be the vibrational ground state of $|g\rangle$. Without loss of generality, we do not take the static disorder into account, which can be included by the ensemble-average of 2DES signals simulated from different initial conditions (i.e., the electronic energy gap) sampled from a Gaussian distribution.[39]

TABLE I. Parameters for the system Hamiltonian of the model two-level system.

Parameters	Value
ω_{eg}[a]	5000 cm^{-1}
ω_0	500 cm^{-1}
S[b]	0.8

[a] $\omega_{eg} = (\epsilon_e - \epsilon_g)/\hbar$.

[b] The displacement with respect to the ground-state equilibrium position d is characterized by the Huang–Rhys factor $S = \omega_0 d^2/2\hbar$.

Numerically, we adopt a finite basis representation (FBR) that includes a truncated set of vibrational eigenstates on each electronic potential energy surface (Gauss–Hermite functions). Note that although we adopt the GWA to derive the friction operator in the QLE approach, the final equation of motion [Eq. (19)] is not limited to a certain nuclear basis. For the harmonic model system studied in this work, we adopt the FBR because it is straightforward for the interpretation of simulated spectra. In general, one can choose other basis representations or Ansätze, such as Gaussian functions and multi-configuration time-dependent Hartree (MCTDH) methods,[60] to implement the QLE approach. Denote the vibrational eigenstates of electronic ground and excited states as $|\alpha_g\rangle$ and $|\alpha_e\rangle$, respectively, and define a short-hand notation $|n,\alpha\rangle = |n\rangle\otimes|\alpha_n\rangle$, where $n = g, e$. The matrix representation of the total Hamiltonian in the FBR can be obtained,

$$\begin{aligned} H(t) &= H_s + F(t) + H_{int}(t) \\ &= H_s + F_g(t) + F_e(t) - \sum_{a=1}^{3} V_a^{(\dagger)}(t), \end{aligned} \tag{67}$$

$$\begin{aligned} H_s = &\sum_\alpha\left[\epsilon_g + \hbar\omega_0\left(\alpha + \frac{1}{2}\right)\right]|g,\alpha\rangle\langle g,\alpha| \\ &+ \sum_\alpha\left[\epsilon_e + \hbar\omega_0\left(\alpha + \frac{1}{2}\right)\right]|e,\alpha\rangle\langle e,\alpha|, \end{aligned} \tag{68}$$

$$\begin{aligned} F_g(t) = &\sqrt{\frac{\hbar}{2\omega_0}}\sum_\alpha\sum_{\alpha'}\Big[\Gamma_g(t)\sqrt{\alpha'+1}\,\delta_{\alpha,\alpha'+1} \\ &+ \Gamma_g(t)\sqrt{\alpha'}\,\delta_{\alpha,\alpha'-1} - \tilde{\Gamma}_g(t)\delta_{\alpha,\alpha'}\Big]|g,\alpha\rangle\langle g,\alpha'|, \end{aligned} \tag{69}$$

$$\begin{aligned} F_e(t) = &\sqrt{\frac{\hbar}{2\omega_0}}\sum_\alpha\sum_{\alpha'}\Big[\Gamma_e(t)\sqrt{\alpha'+1}\,\delta_{\alpha,\alpha'+1} \\ &+ \Gamma_e(t)\sqrt{\alpha'}\,\delta_{\alpha,\alpha'-1} - \tilde{\Gamma}_e(t)\delta_{\alpha,\alpha'}\Big]|e,\alpha\rangle\langle e,\alpha'|, \end{aligned} \tag{70}$$

$$\begin{aligned} V_a(t) = &I_a e^{-4\ln 2\frac{(t-\tau_a)^2}{\tau_p^2}} e^{-i\omega_a(t-\tau_a)}\mu_{ge} \\ &\times\sum_\alpha\sum_{\alpha'}\mathcal{S}_{\alpha,\alpha'}|g,\alpha\rangle\langle e,\alpha'|, \end{aligned} \tag{71}$$

$$\begin{aligned} \mathcal{S}_{\alpha,\alpha'} = &e^{-\frac{S}{2}}\sum_{i=0}^{\alpha}\sum_{j=0}^{\alpha'}\frac{(-1)^j S^{\frac{i+j}{2}}}{i!j!} \\ &\times\sqrt{\frac{\alpha!\alpha'!}{(\alpha-i)!(\alpha'-j)!}}\,\delta_{\alpha-i,\alpha'-j}. \end{aligned} \tag{72}$$

Here, $\mathcal{S}_{\alpha,\alpha'} = \langle\alpha|\alpha'\rangle$ is the Franck–Condon overlap integral between the αth vibrational eigenstate of $|g\rangle$ and the α'th vibrational eigenstate of $|e\rangle$. Note that this representation is already the nuclear eigenstate representation with respect to each electronic potential energy surface, and therefore, the constructed Hamiltonian would be block-diagonalized in each electronic state. The only transitions possible are electronic transitions induced by the field–matter interactions [Eq. (71)] and vibrational transitions induced by the friction operator [Eqs. (69) and (70)].

B. Dissipative wave packet dynamics

To demonstrate the ability of our method to describe the effects of a dissipative environment, we simulated the wave packet dynamics after the model system (Table I) undergoes an excitation by a laser pulse with central frequency $\omega = \omega_{eg} + (S - 1/2)\omega_0 = 5150\,\mathrm{cm}^{-1}$ (vertical transition), and FWHM = 20 fs. Note that the initial wave packet is prepared at $|g, 0\rangle$. The time evolution of the expectation value of the position for the excited-state wave packet at different friction coefficients η is shown in Fig. 1. Note that in Fig. 1, the zero time is set to be the pulse central time. After the excitation by an external field, the excited-state wave packet is generated and evolves on the excited-state potential energy surface. Due to the finite-width pulse, the excitation of the ground-state wave packet and the evolution of the excited-state wave packet occurred simultaneously and continuously before the pulse central time ($t = 0$) is reached, and as a result, the initial value of r_e/d deviates from the Franck–Condon point ($r_e/d = -1$). The expectation value of the position corresponds to the center of the wave packet and varies in time as a damped oscillation. In addition, as the strength of friction increases, as shown in Figs. 1(a)–1(d), the damping is more pronounced. The attenuation of oscillation implies that the friction operator can describe the dissipative dynamics induced by a condensed-phase environment.

Moreover, in Fig. 1, we also compared the dynamics with and without the inclusion of random forces at an ambient temperature (300 K). The inclusion of random forces does not affect the overall dynamics significantly because the relaxation of the excited-state wave packet from vibrational excited states is dominant in the photo-induced dynamics investigated here. We observe that even in a highly dissipative environment, the magnitude of thermal fluctuation at ambient temperature is much smaller than the energy gaps between the low-lying excited states of the system such that the contribution from thermally activated dynamics is negligible. Although the random forces might contribute to the dephasing of

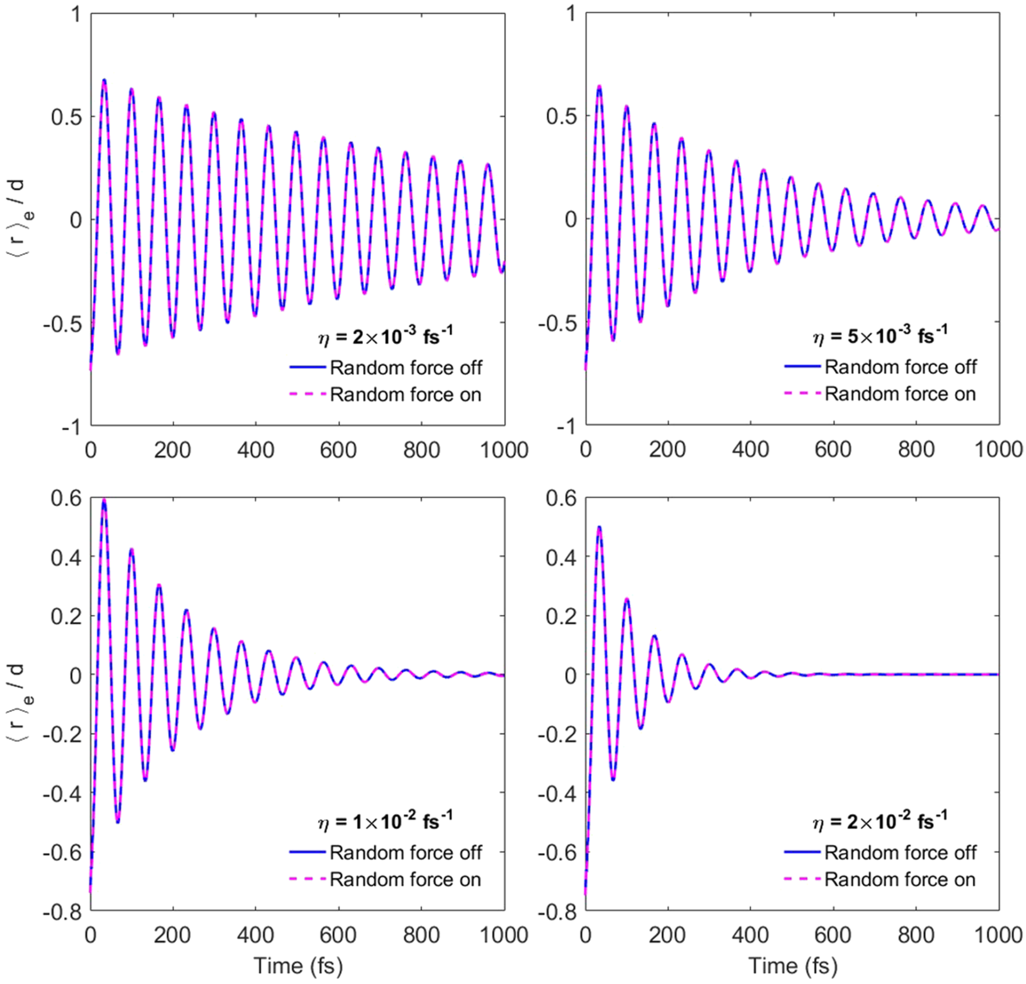

FIG. 1. The time-dependent expectation value of the position for the excited-state wave packet after excitation by a laser pulse. Dynamics simulated at four different friction coefficients (η) are shown. In addition, the solid line corresponds to the results from the simulation without the inclusion of random forces, and the dashed line represents the results obtained from the simulation with the inclusion of random forces and averaged over 500 trajectories.

electronic coherence, in the specific model studied here, dissipation dominates and vibrational coherence is nearly unaffected by the random forces. Based on the above discussions, our results justified that the effects of random forces are not significant in the simulations of dissipative photo-induced dynamics under ambient temperature for the model studied here. This should be valid for model systems in which the vibrational relaxation within a potential energy surface involves vibrational quanta much larger than the thermal energy, resulting in negligible thermally activated uphill vibrational transitions. Therefore, in this study, the 2DES spectra reported in the following were simulated without the inclusion of random forces.

The importance of the random force term in a Schrödinger–Langevin equation approach has been investigated previously,[54] and it was concluded that the QLE approach could still adequately describe non-equilibrium dissipative dynamics without explicitly including the random force term. Moreover, a previous study also showed that a Schrödinger equation with friction can be derived from a quantum trajectory perspective to describe the quantum dissipative dynamics of various models. While details about the regimes where the random force term could be safely neglected must be further investigated, we are confident that the random force does not play a significant role in the dynamics and 2DES spectra simulated in this work.

C. Simulated 2DES spectra

To investigate the effects of a dissipative environment on 2DES spectra, we have simulated 2DES spectra of the model system under different values of the friction coefficient η from a typical solvent environment with an energy relaxation timescale in picoseconds ($\eta = 2 \times 10^{-3}\ \mathrm{fs}^{-1}$) to a highly dissipative environment ($\eta = 2 \times 10^{-2}\ \mathrm{fs}^{-1}$). For the spectra reported in this work, the initial wave packet is set to be $|g, 0\rangle$ to mimic the thermalized ground state. To illustrate the environmental effects on spectral features, we consider the representative case of $\eta = 1 \times 10^{-2}\ \mathrm{fs}^{-1}$. Figures 2 and 3 show rephasing and non-rephasing spectra at different population times, respectively. Peaks in these spectra exhibit a Lorentzian peak shape, which arises from the rapid relaxation of the environment. It is because the environmental effects are described by the Markovian QLE, and the time evolution of the system is analogous to a particle in harmonic potential undergoing Brownian motion.

In both rephasing and non-rephasing spectra, the diagonal peaks show equally spaced peaks in the excitation frequencies and

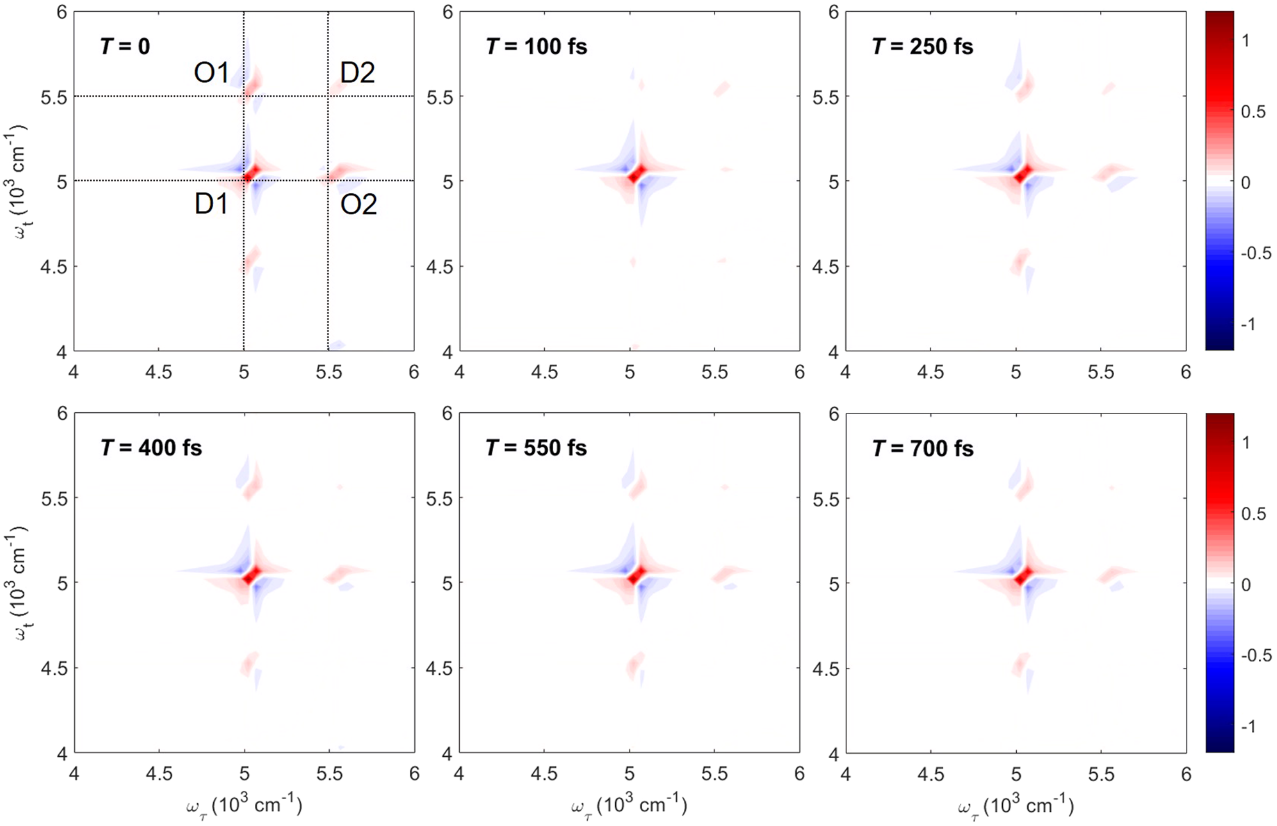

FIG. 2. The real part of simulated rephasing spectra at different population times T $\left(\eta = 1 \times 10^{-2}\mathrm{fs}^{-1}\right)$. The spectra are rescaled by setting the maximum of the rephasing spectrum at T = 0 to be 1. The Lorentzian peak shape arises from the rapid relaxation of the environment. As the population time increases, the decrease in the diagonal peak D2 amplitude describes the vibrational relaxation in the excited state, and the oscillation in peak amplitudes is due to the coherent wave packet dynamics.

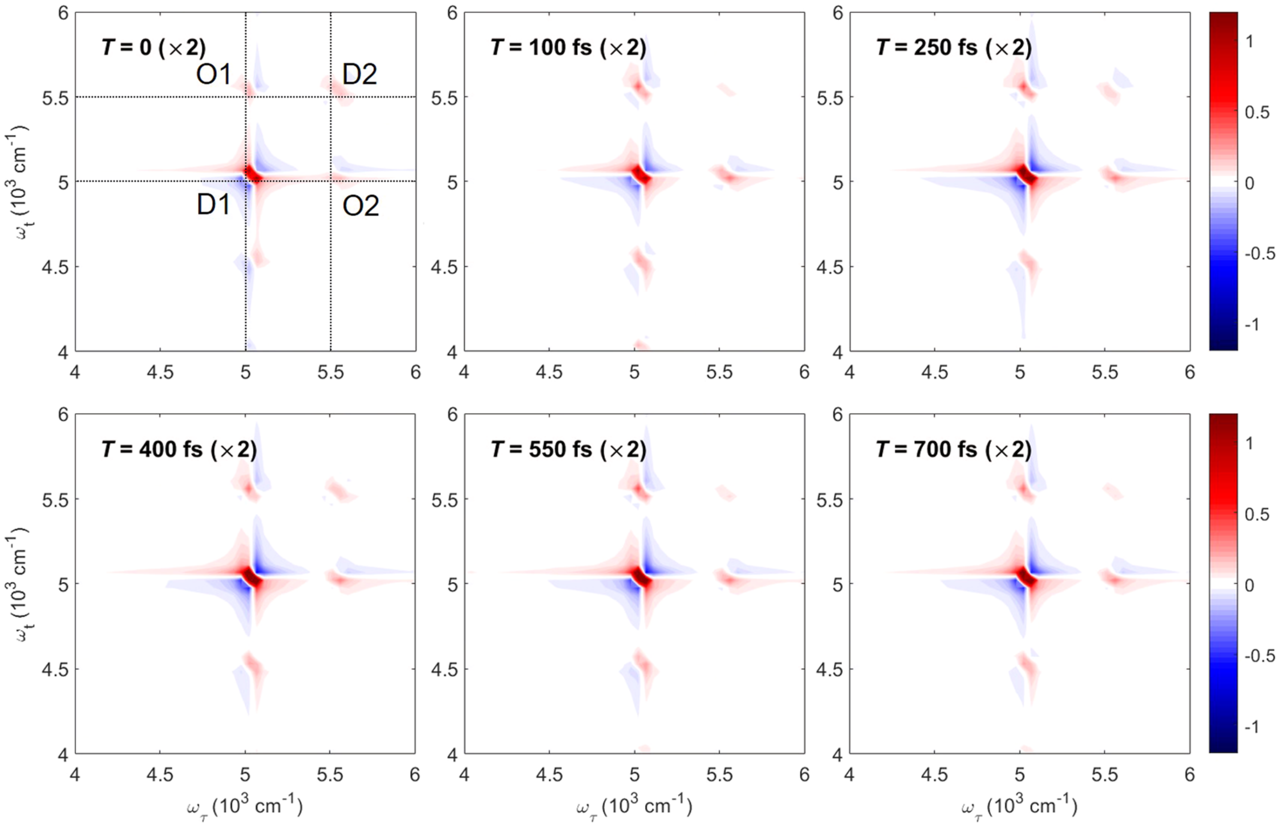

FIG. 3. The real part of non-rephasing spectra at different population times T $\left(\eta = 1 \times 10^{-2}\mathrm{fs}^{-1}\right)$.

an amplitude distribution that is in agreement with the prediction from the Huang–Rhys factor ($S = 0.8$), which resembles the appearance of the vibrational progression corresponding to the linear absorption spectrum. The vertical cut along a specific ω_τ provides information on emission (fluorescence) at a fixed excitation frequency. Given a particular ω_τ, the peaks with $\omega_t < \omega_\tau$ correspond to the Stokes emissions. For example, the peak with $\omega_\tau = 5000$ cm^{-1}, $\omega_t = 4500$ cm^{-1} mainly arises from the pathways that undergo an excitation from $|g, 0\rangle$ to $|e, 0\rangle$ and emit through a $|e, 0\rangle$ to $|g, 1\rangle$ transition. Notice that the overall shape of the 2D spectra is non-symmetric with respect to the horizontal cut along $\omega_t = 5000$ cm^{-1} since the peaks with $\omega_t < 5000$ cm^{-1} are contributed from the Stokes emissions via transitions between the excited state and the high-lying vibrational state in the ground state, which have small transition dipole moments. Moreover, for the labeled diagonal peaks D1 and D2, the decrease in the D2 amplitude accompanies the increase in the D1 amplitude during the population time, and this correlated change in amplitudes can be attributed to the vibrational relaxation in the excited state. In addition, the oscillations in peak amplitudes are indicative of the vibrational coherent dynamics during the population time. The evolution of peak amplitudes will be discussed later.

Notice that at the long population time, the oscillations in peak amplitudes in both rephasing and non-rephasing spectra are attenuated, and in particular, the peak O1 and O2 have similar amplitude and peak shape where the phase patterns are symmetric with respect to the diagonal of the spectra. The similarity between the features of peaks O1 and O2 suggests that these cross peaks mainly reflect the contributions from the GSB pathways at a long population time. The Liouville pathways that may contribute to peaks O1 and O2 at a long population time are shown in Fig. 4. For rephasing spectra, both the GSB pathways that contributed to O1 and O2 are possible. However, the vibrational transfer (VT) pathways have different contributions to O1 and O2. The corresponding pathway for O1 involves the population transfer from $|e, 0\rangle$ to $|e, 1\rangle$ during the population time, which corresponds to the uphill VT and is energetically unfavorable. In contrast, the corresponding pathway for O2 involves the vibrational relaxation from $|e, 1\rangle$ to $|e, 0\rangle$, which is a favorable downhill VT process. Therefore, the VT pathways will have a negligible contribution to O1 such that the amplitude of O1 is solely contributed from the GSB pathways, whereas O2 is contributed from both GSB and VT pathways. Generally speaking, the GSB and VT pathways may have comparable contributions on the cross peaks. In the present model, the contributions of GSB pathways dominate the spectra at a long population time as their overall transition probability, which is related to the magnitude of transition dipole moment in each vibronic transition and the distribution of vibronic-state population, is larger than the overall transition

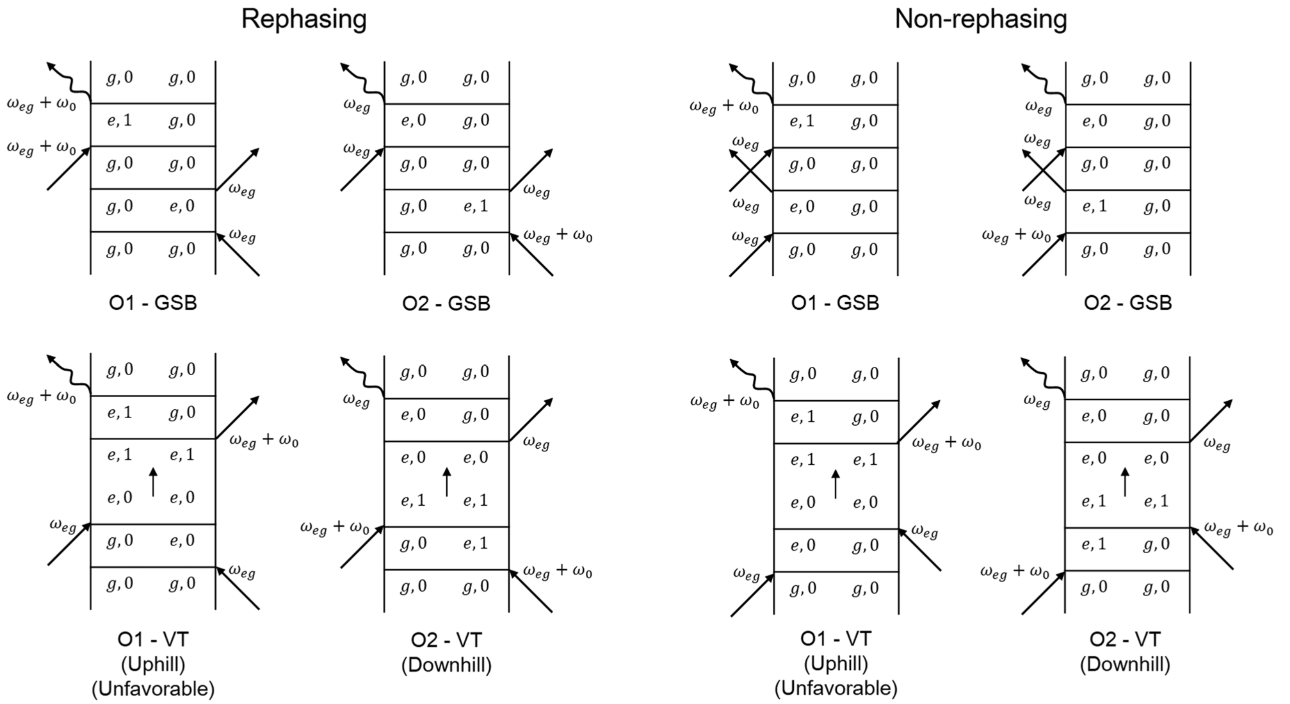

O1 - GSB O2 - GSB O1 - GSB O2 - GSB

O1 - VT (Uphill) (Unfavorable) O2 - VT (Downhill) O1 - VT (Uphill) (Unfavorable) O2 - VT (Downhill)

FIG. 4. Double-sided Feynman diagrams for possible pathways contributed to the cross peaks O1 and O2 at a long population time. The similarity of the peak shape in O1 and O2 mainly results from the GSB pathways instead of the vibrational transfer (VT) pathways that the contributions are related to the excited state population and the direction of VT.

probability of VT pathways. As a result, both peak O1 and O2 are mainly contributed from the GSB pathways and have similar amplitude and peak shape in the long population time. The discussions are the same for the non-rephasing spectra. These observations suggest that the existence of cross peaks may not be a distinctive signature of VT when interpreting the 2DES spectra at a long population time.

D. Vibrational relaxation

To elucidate the effects of a dissipative environment on the vibrational dynamics and the corresponding spectroscopic signals, the evolution of the peak amplitude during the population time is further analyzed. Figure 5 shows that the peak amplitudes of the labeled peaks in rephasing spectra (Fig. 2) vary in population time. Considering diagonal peaks D1 and D2, the amplitude of D1 increases as a function of population time, whereas the amplitude of D2 decreases. Moreover, the decay rate of D2 increases with the increase in the strength of friction. The results suggest that the decrease in the D2 amplitude is due to the vibrational relaxation in the excited state. The peak D2 corresponds to the excitation from $|g,0\rangle$ to $|e,1\rangle$, and therefore, the D2 amplitude is related to the population of $|e,1\rangle$. Under the dissipative environment, the vibrational relaxation from $|e,1\rangle$ to $|e,0\rangle$ during the population time is allowed, and the decrease in $|e,1\rangle$ population leads to the decrease in the D2 amplitude. Therefore, the decrease in the D2 amplitude provides a signature of vibrational relaxation.

More interestingly, the increase in the D1 amplitude suggests the existence of coherence to population transfer. As illustrated in Fig. 6, the excited-state coherence transfer during the population time leads to the increase in $|e,0\rangle$ population, which increases the D1 amplitude. Moreover, the increase in the D1 amplitude is more significant when the strength of friction is weaker, which implies that for the slower decoherence rate, the coherence transfer in the excited state is more likely to occur, consistent with our discussions. Similar features of the evolution of diagonal peak amplitudes are observed in the non-rephasing spectra. As shown in Fig. 7, the increase in the D1 amplitude can be attributed to the coherence transfer on the electronic excited state.

The decay in diagonal peak amplitudes implies that the QLE approach successfully describes the vibration relaxation dynamics in a condensed-phase environment. In addition, the coherence transfer pathways, which are often neglected in Redfield-theory based methods with secular approximation to preserve the positivity, are naturally involved in our wavefunction based method. In addition, conventionally, the cross peaks, especially the one in the lower diagonal (e.g., peak O2), are considered to be the signature of VT. However, following the discussions on Fig. 2 about the peak shapes of cross peaks O1 and O2 in the long population time, the cross peaks are mainly contributed from GSB instead of VT. Hence, our computational results suggest that the spectral features of VT are less obvious by solely observing the existence of cross peaks.

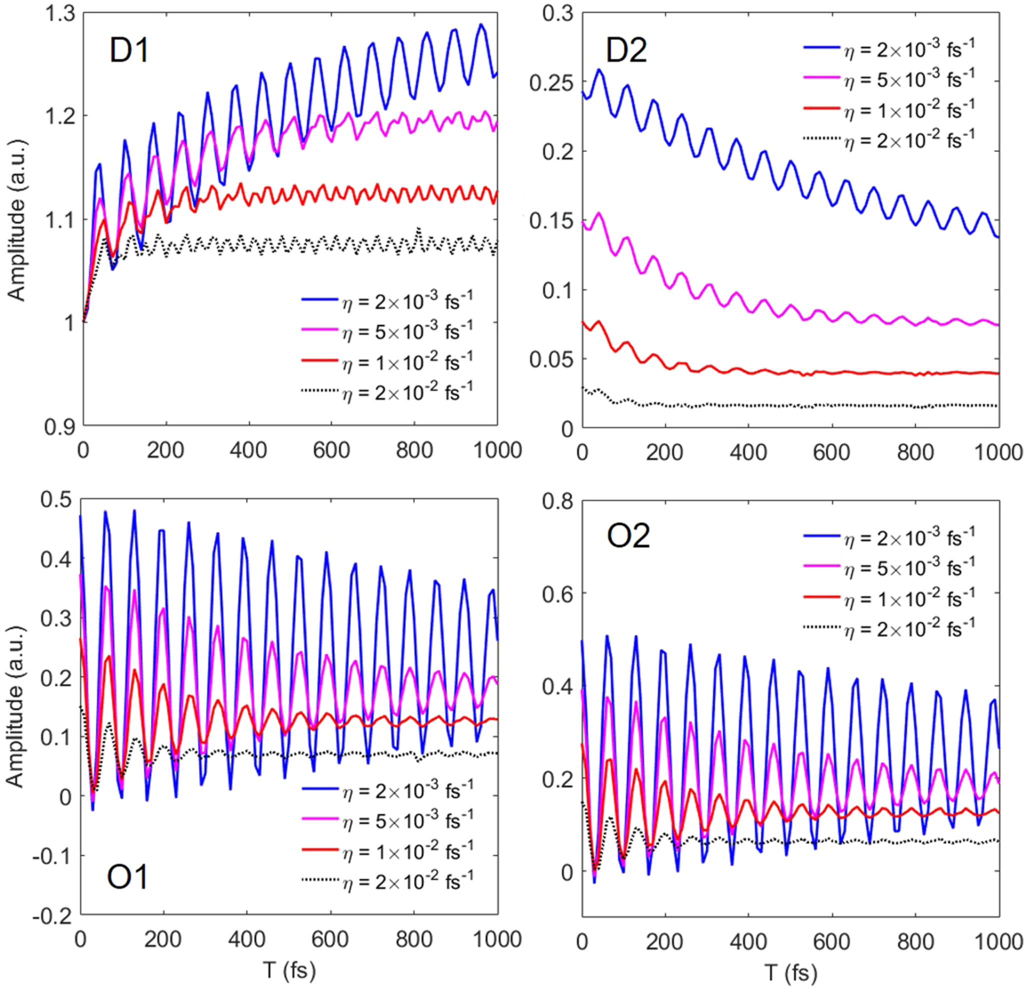

FIG. 5. The time evolution of the amplitude of the labeled peak in rephasing spectra (Fig. 2) under different strengths of friction. The vibrational relaxation, coherence transfer, and decoherence induced by a dissipative environment manifest the decrease in the D2 amplitude, the increase in the D1 amplitude, and the attenuation of quantum beats, respectively.

E. Vibrational quantum beating

As shown in Fig. 5, the evolution of peak amplitudes in the population time is associated with a quantum beating. The beating in amplitude has the same frequency as the vibration frequency ω_0 of the system, which implies that the amplitude oscillation manifests the vibrational coherence. Moreover, the beating amplitude attenuates as the population time increases, and the decay in the amplitude is faster as the strength of friction increases. The change in the beating amplitude corresponds to the decoherence of the system under a dissipative environment. The results indicate that the QLE approach can describe the transition between coherent and incoherent wave packet dynamics.

The beating in peak amplitude consists of both ground-state and excited-state vibrational coherences that arise from the wave packet dynamics within an electronic state. In Fig. 5, an out-of-phase oscillation between the amplitude of diagonal peaks with respect to the cross peaks is observed. To elucidate the origin of the observed vibrational quantum beatings, we further analyze the coherence pathways that associated with each peak. The coherence pathways contributing to the labeled peaks in rephasing spectra are shown in Fig. 8. For each labeled peak, we list the major excited-state coherence (ESC) and ground-state coherence (GSC) pathways and their transition dipole strengths defined by the product of transition dipole moments of vibronic transitions, which can be regarded as weightings of each pathway contribution. Under the Condon approximation, the transition dipole moment is proportional to the Franck–Condon factor. We first focus on the cross peaks O1 and O2. For peak O1, the vibrational coherence in the ESC pathway is out-of-phase relative to the one in GSC pathways such that the beating from different pathways partially cancels out. Within the model system we studied in this work, the Huang–Rhys factor $S < 1$ such that the transition dipole strength of ESC pathways is larger than the one of the GSC pathways and the beating in peak O1 is the net contribution

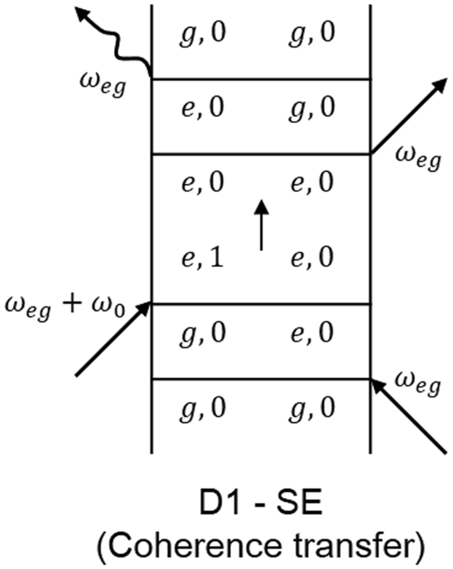

D1 - SE
(Coherence transfer)

FIG. 6. The Liouville pathway accounts for the increase in the D1 amplitude. The increase in the amplitude can be attributed to the excited-state coherence transfer process.

from ESC. For peak O2, the vibrational coherences in both ESC and GSC pathways are in-phase and the beating is the sum of them. Due to the larger transition dipole strength of ESC, the observed beating in peak O2 is dominated by the ESC contribution. Therefore, the ESC is dominant in the vibrational quantum beating in peaks O1 and O2, which suggests that the cross peaks can provide the ESC information.

Next, for both diagonal peaks D1 and D2, the vibrational coherence between the ESC and GSC pathways is out-of-phase. However, both coherence pathways have the same transition dipole strength such that one cannot determine directly which pathway is dominant. Note that normally, the decoherence of ESC, such as $|e,1\rangle\langle e,0|$ and $|e,2\rangle\langle e,1|$, would be faster than the GSC and is indeed found so in our trace in Fig. 5. Based on the observation of the out-of-phase oscillation between diagonal and cross-peak amplitudes and the previous discussion that the beating in peak O1 is dominated by ESC, we suggest that the GSC is dominant in the beating in diagonal peaks. Therefore, based on our model calculations, the diagonal peaks and cross peaks can provide information of GSC and ESC, respectively. The results suggest that 2DES could be an effective probe for distinguishing ESC and GSC, which is useful for probing different potential energy surfaces in different electronic states. These general principles provide a powerful basis for observing vibrational coherences on different electronic potential energy surfaces via the 2DES

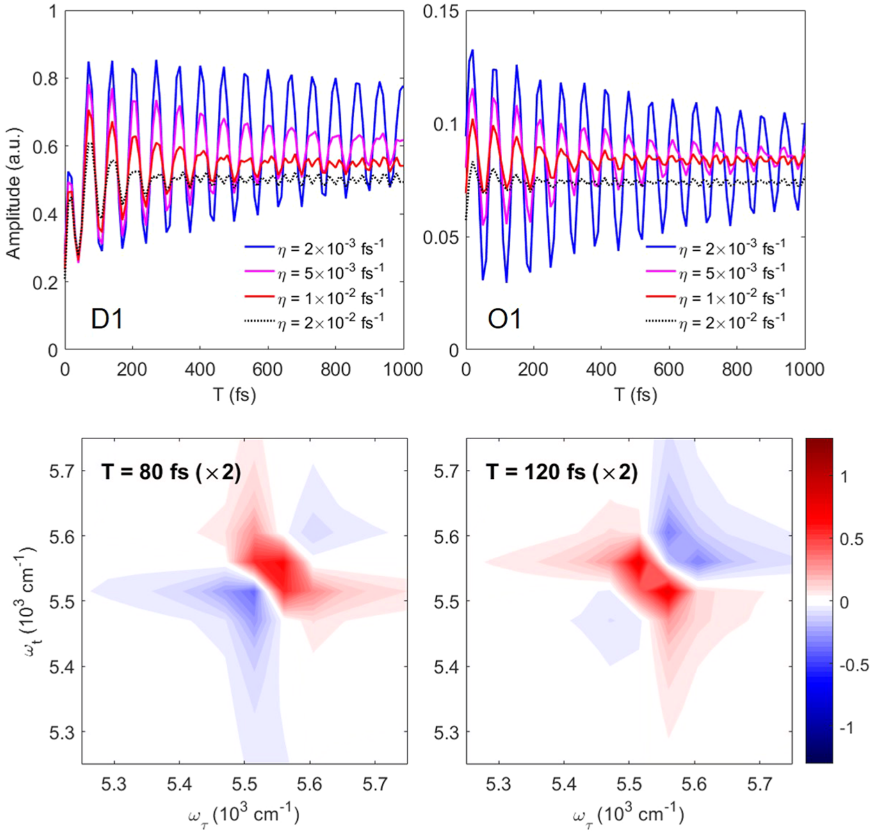

FIG. 7. Top row: the time evolution of the amplitude of the labeled peak in non-rephasing spectra (Fig. 3) under different strengths of friction. Bottom row: the peak shape change in D2 in non-rephasing spectra along the population time (η = 2 × 10^{-3} fs^{-1}). The phase-flipping suggests that the amplitude of D2 is dominated by coherence pathways.

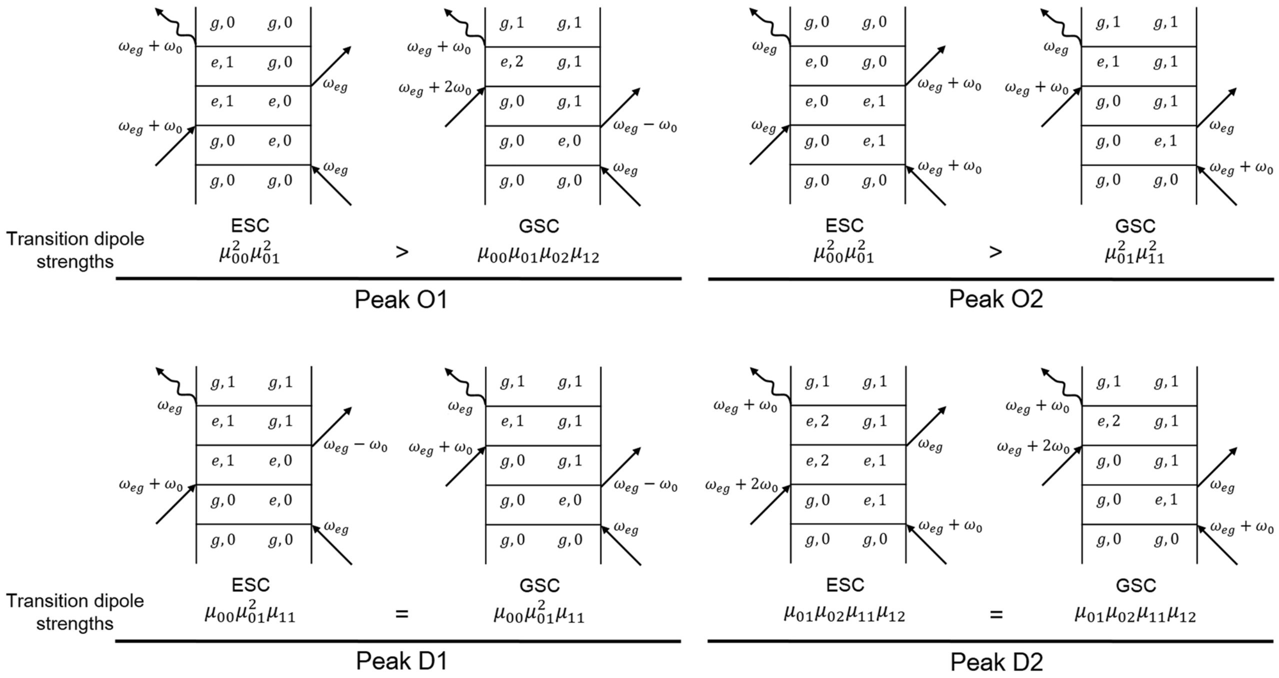

FIG. 8. Double-sided Feynman diagrams for the major coherence pathways contributing to the labeled peaks in rephasing spectra. The vibrational quantum beating in 2DES signals contains information on both excited-state coherence (ESC) and ground-state coherence (GSC). For peaks D1, D2, and O1, the ESC and GSC are out-of-phase, whereas the ESC and GSC are in-phase for peak O2. The transition dipole strength, defined as the product of transition dipole moments, is used to determine the relative contribution of ESC and GSC pathways. In contrast to the beatings in cross peaks that are dominated by ESC, the transition dipole strengths alone cannot determine which type of coherence is dominant in the diagonal peaks.

technique. However, we only investigated a simple displaced harmonic oscillator model in this work. For more complex systems, additional considerations might be needed in order to accurately interpret vibronic quantum beating signals on 2DES spectra.

In addition to the signals in rephasing spectra, the oscillation in peak amplitudes is also observed in non-rephasing spectra (Fig. 7), where the attenuation of the beating amplitude arises from the decoherence induced by the environment. In contrast to rephasing spectra, the signal contributed from the pathways that involve vibrational coherence is shown to be more pronounced in the case of non-rephasing spectra such that the increase in the D1 amplitude is less significant. Comparing the evolution of the peak amplitude in rephasing (Fig. 5) and non-rephasing spectra, the oscillations in signals of non-rephasing spectra have a phase shift of π with respect to the signals in rephasing spectra. The phase shift is due to the reverse order of interactions between the first two pulses in a non-rephasing condition. Furthermore, the coherent dynamics of the system leads to the change in the peak shape of D2 in non-rephasing spectra (Fig. 7). Under the condition of weak friction strength, the peak shape of D2 shows a periodic change during the population time until the decoherence is completed. As shown in Fig. 7, the change in the peak shape, which corresponds to flipping with respect to the anti-diagonal line and the sign change in the amplitude at the peak center, implies that the coherence pathways have dominant contributions to the D2 amplitude. Overall, the simulated spectra demonstrated that the QLE approach can reproduce the spectral features that arise from vibrational relaxation and decoherence in both rephasing and non-rephasing conditions.

F. Remarks on the QLE approach

Based on the simulated 2DES spectra, we suggest that it is sufficient to simulate the spectroscopic signals in a dissipative environment at ambient temperature by only considering the effects of frictional forces on the wave packet dynamics. As mentioned in Sec. III B, the random forces will not have significant effects on the wave packet dynamics of a photo-induced process in the condensed phase as the magnitude of thermal fluctuations is much smaller than the energy scale of the vibronic excitations. The spectral and temporal evolutions of the 2DES signals reported in this section show that even the random forces are neglected in the simulations, the dissipative wave packet dynamics and the corresponding manifestations in spectra are well described by the QLE approach. Therefore, a single-trajectory simulation of 2DES spectra using the QLE approach is enough to describe the dynamical and spectroscopic behavior of a molecular system in the condensed phase when the static disorder is omitted. Even with the inclusion of static disorder, the number of trajectories needed for the ensemble average can be reduced to a small value by using an efficient sampling scheme. In this regard, the QLE approach has a relatively low computational cost compared with the density-matrix based methods such that it provides an efficient tool for studying the dynamics and the nonlinear optical responses of molecular systems, especially the one with strong vibronic couplings.

Finally, we note that although a displaced harmonic oscillator model is studied in this work, the QLE approach developed here is not limited to harmonic systems. Models with more complicated potential energy surfaces can be simulated efficiently using available wave packet propagation methods.[61] Moreover, the QLE approach is not restricted to a particular choice of basis representation. The method presented in this work can be applied to a system with the Hamiltonian parameterized by *ab initio* calculations once a suitable basis is chosen (e.g., a discrete variable representation[61]). Therefore, the QLE approach is capable of fully exploring coupled electronic-vibrational motions in complex molecular systems.

IV. CONCLUSIONS

In this study, we have proposed a QLE based method for the simulations of 2DES spectra in a condensed-phase environment. For the numerical implementation of QLE, we generalized the friction operator based algorithm proposed by Messina and co-workers for a multi-dimensional system. To demonstrate the applicability of our method, we have simulated the rephasing and non-rephasing spectra of a displaced-oscillator model in a dissipative environment. With the explicit treatment of vibrational relaxation in quantum wave packet dynamics simulations, the QLE approach successfully describes vibrational relaxation, coherence transfer, and decoherence in dissipative wave packet dynamics, as well as their corresponding spectral features.

We emphasize that in the simulated spectra, the capability of the QLE approach in providing insight into the role of vibrational relaxation and coherence transfer is demonstrated in the evolutions of spectroscopic signals under the influence of an environment. Based on the wavefunction based simulations, the relation between the observed beating in the peak amplitude and the coherent wave packet dynamics in different electronic states can be elucidated, from which we suggest that there may be a possibility of separating ground-state and excited-state wave packet dynamics from 2DES data. The decay in vibrational quantum beating due to a condensed-phase environment is naturally described by the QLE approach. With the correct description of vibrational decoherence, it is possible to analyze the features of the 2DES spectra at a long-population time, where we suggest that the cross peaks below the diagonal of the spectra may not be an unambiguous signature of vibrational relaxation as the contributions of both GSB and VT pathways are comparable. Overall, the computational results suggest that the 2DES technique could be a sensitive probe for the vibrational relaxation, coherence transfer, and decoherence in dissipative wave packet dynamics. Note that such interpretations of vibrational quantum beating on 2DES signals have drawn intense research activities.[7,10,12,15,16,19–22] Nevertheless, our simulations provide clear elucidations of spectral signatures and clear interpretations of GSC and ESC in 2DES signals, which could be a valuable addition to the power of 2DES.

Compared with the response-function based methods, the QLE approach allows full dynamical simulation of 2DES spectra, including the pulse-overlap effects, Liouville pathways arising from dissipative dynamics, and interference between different Liouville pathways. Moreover, molecular systems are often found with intricate couplings between electronic and vibrational degrees of freedom, and it is necessary to consider all relevant degrees of freedom to study the photo-induced dynamics and the corresponding spectroscopic signals. Numerically, the number of basis states inevitably grows rapidly as the dimensionality of the system increases. Our results justify that for the photo-induced process in the condensed phase, the environmental effects can be well described once the frictional force experienced by the system is properly treated. As the random forces can be reasonably neglected, the number of trajectories can be significantly reduced such that the QLE approach, which explicitly treats the nuclear wave packet dynamics, is more efficient than the density-matrix based methods, especially for a multi-dimensional system described by a large number of basis states. Therefore, the QLE approach proposed in this work may provide an efficient tool to simulate the 2DES spectra with both electronic and vibrational degrees of freedom being resolved, especially for the multi-dimensional system.

In addition, our method can provide an effective tool for theoretical studies on vibrationally resolved 2D spectroscopy (e.g., 2DEV) and the spectral signatures manifested by vibronic couplings. Since full wave packet dynamics are evolved in our simulations, the method presented in this work is not limited to systems with harmonic potentials. Anharmonic systems or potentials obtained from *ab initio* calculations can be easily simulated within the same framework, which significantly expands the scope of the problems that can be studied. Note that in the QLE approach, the effects of a dissipative environment are represented by a friction operator, which has a simple functional form and is easy to implement numerically. Although we have limited our discussions to the effects of Markovian friction, it can be readily extended to study the non-Markovian dynamics by replacing the constant friction coefficient into the friction kernel and the corresponding fluctuation–dissipation relation for the random forces. Furthermore, the QLE approach can be used to simulate linear and other nonlinear optical responses by suitable modifications of the field–matter interaction Hamiltonian.

ACKNOWLEDGMENTS

Y.-C.C. thanks the Ministry of Science and Technology, Taiwan (Grant No. MOST 109-2113-M-002-004), and National Taiwan University (Grant No. 109L892005) for financial support. We are acknowledge the Computer and Information Networking Center, National Taiwan University, for providing access to high-performance computing facilities. We thank the National Center for High-Performance Computing for the computer time and facilities.

APPENDIX: DERIVATION OF PERTURBATIVE CONTRIBUTIONS

Note that the wavefunction evolved by Eq. (29) contains contributions from all perturbative orders of field–matter interactions. In order to extract the third-order photon-echo signals, contributions with desired order of interactions (i.e., first order in each pulse) in Eq. (28) must be evaluated. To this end, we consider the wavefunction as a function of electric field strength of each laser pulse (λ_1, λ_2,

λ_3) and define the perturbative expansion[37] with respect to (λ_1, λ_2, λ_3),

$$\begin{aligned}&\left|\psi_{a(\dagger)b(\dagger)c(\dagger)}(t)\right\rangle\\&\quad=\sum_{i,j,k=0}^{\infty}\left[\lambda_{1(\dagger)}^{i}\right]^{a}\left[\lambda_{2(\dagger)}^{j}\right]^{b}\left[\lambda_{3(\dagger)}^{k}\right]^{c}\left|\psi_{a(\dagger)b(\dagger)c(\dagger)}^{(i\cdot a+j\cdot b+k\cdot c)}(t)\right\rangle\\&\quad\equiv\sum_{i,j,k=0}^{\infty}\lambda_{1(\dagger)}^{i\cdot a}\lambda_{2(\dagger)}^{j\cdot b}\lambda_{3(\dagger)}^{k\cdot c}\left|(i\cdot a)(j\cdot b)(k\cdot c)\right\rangle.\end{aligned}\tag{A1}$$

Here, $|(i\cdot a)(j\cdot b)(k\cdot c)\rangle$ is a shorthand notation for the perturbative $\left|\phi_{a(\dagger)b(\dagger)c(\dagger)}^{(i\cdot a+j\cdot b+k\cdot c)}(t)\right\rangle$ term. Equation (A1) indicates that these $\left|\phi_{a(\dagger)b(\dagger)c(\dagger)}^{(i\cdot a+j\cdot b+k\cdot c)}(t)\right\rangle$ terms can be related to $|\psi_{a(\dagger)b(\dagger)c(\dagger)}(t)\rangle$ terms. In other words, we can utilize wavefunctions evolved by Eq. (29) as auxiliary wavefunctions to generate contributions with a specific order of interactions. Moreover, at the weak-field condition for the common four-wave mixing experiments, the expansion can be truncated at a low order of λ. We introduce the following auxiliary wavefunctions and expand them according to Eq. (A1):

$$\begin{aligned}\langle\psi_{11^\dagger0}(t)|&=\sum_{i,j=0}^{\infty}\lambda_1^i\lambda_{2^\dagger}^j\langle ij0|\\&=\langle000|+\lambda_1\langle100|+\lambda_{2^\dagger}\langle010|+\lambda_1^2\langle200|\\&\quad+\lambda_{2^\dagger}^2\langle020|+\lambda_1\lambda_{2^\dagger}\langle110|\\&\quad+\mathcal{O}\left(\lambda_1^i\lambda_{2^\dagger}^j,i+j\geq3\right),\end{aligned}\tag{A2}$$

$$\begin{aligned}\langle\psi_{101^\dagger}(t)|&=\sum_{i,k=0}^{\infty}\lambda_1^i\lambda_{3^\dagger}^k\langle i0k|\\&=\langle000|+\lambda_1\langle100|+\lambda_{3^\dagger}\langle001|+\lambda_1^2\langle200|\\&\quad+\lambda_{3^\dagger}^2\langle002|+\lambda_1\lambda_{3^\dagger}\langle101|+\mathcal{O}\left(\lambda_1^i\lambda_{3^\dagger}^k,i+k\geq3\right),\end{aligned}\tag{A3}$$

$$\begin{aligned}\langle\psi_{100}(t)|&=\sum_{i=0}^{\infty}\lambda_1^i\langle i00|\\&=\langle000|+\lambda_1\langle100|+\mathcal{O}\left(\lambda_1^i,i\geq2\right),\end{aligned}\tag{A4}$$

$$\begin{aligned}\langle\psi_{000}(t)|&=\langle000|,\\|\psi_{11^\dagger1^\dagger}(t)\rangle&=\sum_{i,j,k=0}^{\infty}\lambda_1^i\lambda_{2^\dagger}^j\lambda_{3^\dagger}^k|ijk\rangle\\&=|000\rangle+\lambda_1|100\rangle+\lambda_{2^\dagger}|010\rangle+\lambda_{3^\dagger}|001\rangle+\lambda_1^2|200\rangle\\&\quad+\lambda_{2^\dagger}^2|020\rangle+\lambda_{3^\dagger}^2|002\rangle+\lambda_1\lambda_{2^\dagger}|110\rangle+\lambda_1\lambda_{3^\dagger}|101\rangle\\&\quad+\lambda_{2^\dagger}\lambda_{3^\dagger}|011\rangle+\lambda_1^3|300\rangle+\lambda_{2^\dagger}^3|030\rangle+\lambda_{3^\dagger}^3|003\rangle\\&\quad+\lambda_1^2\lambda_{2^\dagger}|210\rangle+\lambda_1^2\lambda_{3^\dagger}|201\rangle+\lambda_1\lambda_{2^\dagger}^2|120\rangle+\lambda_{2^\dagger}^2\lambda_{3^\dagger}|021\rangle\\&\quad+\lambda_1\lambda_{3^\dagger}^2|102\rangle+\lambda_{2^\dagger}\lambda_{3^\dagger}^2|012\rangle+\lambda_1\lambda_{2^\dagger}\lambda_{3^\dagger}|111\rangle\\&\quad+\mathcal{O}\left(\lambda_1^i\lambda_{2^\dagger}^j\lambda_{3^\dagger}^k,i+j+k\geq4\right),\end{aligned}\tag{A5}$$

$$\begin{aligned}|\psi_{11^\dagger0}(t)\rangle&=\sum_{i,j=0}^{\infty}\lambda_1^i\lambda_{2^\dagger}^j|ij0\rangle\\&=|000\rangle+\lambda_1|100\rangle+\lambda_{2^\dagger}|010\rangle+\lambda_1^2|200\rangle\\&\quad+\lambda_{2^\dagger}^2|020\rangle+\lambda_1\lambda_{2^\dagger}|110\rangle+\mathcal{O}\left(\lambda_1^i\lambda_{2^\dagger}^j,i+j\geq3\right),\end{aligned}\tag{A6}$$

$$\begin{aligned}|\psi_{101^\dagger}(t)\rangle&=\sum_{i,k=0}^{\infty}\lambda_1^i\lambda_{3^\dagger}^k|i0k\rangle\\&=|000\rangle+\lambda_1|100\rangle+\lambda_{3^\dagger}|001\rangle+\lambda_1^2|200\rangle\\&\quad+\lambda_{3^\dagger}^2|002\rangle+\lambda_1\lambda_{3^\dagger}|101\rangle+\mathcal{O}\left(\lambda_1^i\lambda_{3^\dagger}^k,i+k\geq3\right),\end{aligned}\tag{A7}$$

$$\begin{aligned}|\psi_{01^\dagger1^\dagger}(t)\rangle&=\sum_{j,k=0}^{\infty}\lambda_{2^\dagger}^j\lambda_{3^\dagger}^k|0jk\rangle\\&=|000\rangle+\lambda_{2^\dagger}|010\rangle+\lambda_{3^\dagger}|001\rangle+\lambda_{2^\dagger}^2|020\rangle\\&\quad+\lambda_{3^\dagger}^2|002\rangle+\lambda_{2^\dagger}\lambda_{3^\dagger}|011\rangle+\mathcal{O}\left(\lambda_{2^\dagger}^j\lambda_{3^\dagger}^k,j+k\geq3\right),\end{aligned}\tag{A8}$$

$$\begin{aligned}|\psi_{01^\dagger0}(t)\rangle&=\sum_{j=0}^{\infty}\lambda_{2^\dagger}^j|0j0\rangle\\&=|000\rangle+\lambda_{2^\dagger}|010\rangle+\mathcal{O}\left(\lambda_{2^\dagger}^j,j\geq2\right),\\|\psi_{001^\dagger}(t)\rangle&=\sum_{k=0}^{\infty}\lambda_{3^\dagger}^k|00k\rangle\\&=|000\rangle+\lambda_{3^\dagger}|001\rangle+\mathcal{O}\left(\lambda_{3^\dagger}^k,k\geq2\right),\\|\psi_{000}(t)\rangle&=|000\rangle.\end{aligned}\tag{A9}$$

In addition, using the fact that the electronic ground state cannot be annihilated, the bras and kets in Eq. (28) can then be obtained by the following linear combinations:

$$\begin{aligned}\left\langle\phi_{100}^{(1)}(t)\right|&=\lambda_1\langle100|\\&=\langle\psi_{100}(t)|-\langle\psi_{000}(t)|,\end{aligned}\tag{A10}$$

$$\begin{aligned}\left|\phi_{01^\dagger0}^{(1)}(t)\right\rangle&=\lambda_{2^\dagger}|010\rangle\\&=|\psi_{01^\dagger0}(t)\rangle-|\psi_{000}(t)\rangle,\end{aligned}\tag{A11}$$

$$\begin{aligned}\left|\phi_{001^\dagger}^{(1)}(t)\right\rangle&=\lambda_{3^\dagger}|001\rangle\\&=|\psi_{001^\dagger}(t)\rangle-|\psi_{000}(t)\rangle,\end{aligned}\tag{A12}$$

$$\begin{aligned}\left\langle\phi_{11^\dagger0}^{(2)}(t)\right|&=\lambda_1\lambda_{2^\dagger}\langle110|\\&=\langle\psi_{11^\dagger0}(t)|-\langle\psi_{100}(t)|,\end{aligned}\tag{A13}$$

$$\begin{aligned}\left\langle\phi_{101^\dagger}^{(2)}(t)\right|&=\lambda_1\lambda_{3^\dagger}\langle101|\\&=\langle\psi_{101^\dagger}(t)|-\langle\psi_{100}(t)|,\end{aligned}\tag{A14}$$

$$\begin{aligned}\left|\phi_{01^\dagger1^\dagger}^{(2)}(t)\right\rangle&=\lambda_{2^\dagger}\lambda_{3^\dagger}|011\rangle\\&=|\psi_{01^\dagger1^\dagger}(t)\rangle-|\psi_{01^\dagger0}(t)\rangle-|\psi_{001^\dagger}(t)\rangle+|\psi_{000}(t)\rangle,\end{aligned}\tag{A15}$$

$$
\begin{aligned}
\left|\phi^{(3)}_{11^\dagger 1^\dagger}(t)\right\rangle &= \lambda_1\lambda_{2^\dagger}\lambda_{3^\dagger}|111\rangle \\
&= |\psi_{11^\dagger 1^\dagger}(t)\rangle - |\psi_{11^\dagger 0}(t)\rangle - |\psi_{101^\dagger}(t)\rangle - |\psi_{01^\dagger 1^\dagger}(t)\rangle \\
&\quad + |\psi_{01^\dagger 0}(t)\rangle + |\psi_{001^\dagger}(t)\rangle. \qquad \text{(A16)}
\end{aligned}
$$

Thus, terms required in the evaluation of 3PPE polarization [Eq. (28)] can be calculated from auxiliary wavefunctions, as defined in Eqs. (A10)–(A16).

DATA AVAILABILITY

The data that support the findings of this study are available from the corresponding author upon reasonable request.

REFERENCES

[1] J. D. Hybl, A. Albrecht Ferro, and D. M. Jonas, "Two-dimensional Fourier transform electronic spectroscopy," J. Chem. Phys. **115**, 6606–6622 (2001).

[2] W. M. Zhang, V. Chernyak, and S. Mukamel, "Multidimensional femtosecond correlation spectroscopies of electronic and vibrational excitons," J. Chem. Phys. **110**, 5011–5028 (1999).

[3] M. Cho, "Coherent two-dimensional optical spectroscopy," Chem. Rev. **108**, 1331–1418 (2008).

[4] N. S. Ginsberg, Y.-C. Cheng, and G. R. Fleming, "Two-dimensional electronic spectroscopy of molecular aggregates," Acc. Chem. Res. **42**, 1352–1363 (2009).

[5] F. D. Fuller and J. P. Ogilvie, "Experimental implementations of two-dimensional Fourier transform electronic spectroscopy," Annu. Rev. Phys. Chem. **66**, 667–690 (2015).

[6] M. K. Petti, J. P. Lomont, M. Maj, and M. T. Zanni, "Two-dimensional spectroscopy is being used to address core scientific questions in biology and materials science," J. Phys. Chem. B **122**, 1771–1780 (2018).

[7] D. M. Jonas, "Vibrational and nonadiabatic coherence in 2D electronic spectroscopy, the Jahn–Teller effect, and energy transfer," Annu. Rev. Phys. Chem. **69**, 327–352 (2018).

[8] T. A. A. Oliver, "Recent advances in multidimensional ultrafast spectroscopy," R. Soc. Open Sci. **5**, 171425 (2018).

[9] A. Gelzinis, R. Augulis, V. Butkus, B. Robert, and L. Valkunas, "Two-dimensional spectroscopy for non-specialists," Biochim. Biophys. Acta, Bioenerg. **1860**, 271–285 (2019).

[10] L. Wang, M. A. Allodi, and G. S. Engel, "Quantum coherences reveal excited-state dynamics in biophysical systems," Nat. Rev. Chem. **3**, 477–490 (2019).

[11] F. Milota, J. Sperling, A. Nemeth, T. Mančal, and H. F. Kauffmann, "Two-dimensional electronic spectroscopy of molecular excitons," Acc. Chem. Res. **42**, 1364–1374 (2009).

[12] F. Milota, V. I. Prokhorenko, T. Mancal, H. von Berlepsch, O. Bixner, H. F. Kauffmann, and J. Hauer, "Vibronic and vibrational coherences in two-dimensional electronic spectra of supramolecular J-aggregates," J. Phys. Chem. A **117**, 6007–6014 (2013).

[13] C. L. Smallwood and S. T. Cundiff, "Multidimensional coherent spectroscopy of semiconductors," Laser Photonics Rev. **12**, 1800171 (2018).

[14] P. Nuernberger, S. Ruetzel, and T. Brixner, "Multidimensional electronic spectroscopy of photochemical reactions," Angew. Chem., Int. Ed. **54**, 11368–11386 (2015).

[15] F. Fassioli, R. Dinshaw, P. C. Arpin, and G. D. Scholes, "Photosynthetic light harvesting: Excitons and coherence," J. R. Soc. Interface **11**, 20130901 (2014).

[16] A. Chenu and G. D. Scholes, "Coherence in energy transfer and photosynthesis," Annu. Rev. Phys. Chem. **66**, 69–96 (2015).

[17] J. C. Dean and G. D. Scholes, "Coherence spectroscopy in the condensed phase: Insights into molecular structure, environment, and interactions," Acc. Chem. Res. **50**, 2746–2755 (2017).

[18] M. K. Lee, P. Huo, and D. F. Coker, "Semiclassical path integral dynamics: Photosynthetic energy transfer with realistic environment interactions," Annu. Rev. Phys. Chem. **67**, 639–668 (2016).

[19] F. Ma, E. Romero, M. R. Jones, V. I. Novoderezhkin, and R. van Grondelle, "Vibronic coherence in the charge separation process of the *Rhodobacter sphaeroides* reaction center," J. Phys. Chem. Lett. **9**, 1827–1832 (2018).

[20] E. Thyrhaug, R. Tempelaar, M. J. P. Alcocer, K. Žídek, D. Bína, J. Knoester, T. L. C. Jansen, and D. Zigmantas, "Identification and characterization of diverse coherences in the Fenna–Matthews–Olson complex," Nat. Chem. **10**, 780–786 (2018).

[21] S. Rafiq, B. Fu, K. Bryan, and G. D. Scholes, "Interplay of vibrational wavepackets during an ultrafast electron transfer reaction," Nat. Chem. **13**, 70 (2020).

[22] E. A. Arsenault, Y. Yoneda, M. Iwai, K. K. Niyogi, and G. R. Fleming, "Vibronic mixing enables ultrafast energy flow in light-harvesting complex II," Nat. Commun. **11**, 1460 (2020).

[23] T. A. A. Oliver, N. H. C. Lewis, and G. R. Fleming, "Correlating the motion of electrons and nuclei with two-dimensional electronic–vibrational spectroscopy," Proc. Natl. Acad. Sci. U. S. A. **111**, 10061–10066 (2014).

[24] F. Terenziani and A. Painelli, "Two-dimensional electronic-vibrational spectra: Modeling correlated electronic and nuclear motion," Phys. Chem. Chem. Phys. **17**, 13074–13081 (2015).

[25] J. D. Gaynor and M. Khalil, "Signatures of vibronic coupling in two-dimensional electronic-vibrational and vibrational-electronic spectroscopies," J. Chem. Phys. **147**, 094202 (2017).

[26] P. Bhattacharyya and G. R. Fleming, "Two-dimensional electronic–vibrational spectroscopy of coupled molecular complexes: A near-analytical approach," J. Phys. Chem. Lett. **10**, 2081–2089 (2019).

[27] S. Mukamel, *Principles of Nonlinear Optical Spectroscopy* (Oxford University Press, New York, 1995), Vol. 6.

[28] L. Chen, R. Zheng, Q. Shi, and Y. Yan, "Two-dimensional electronic spectra from the hierarchical equations of motion method: Application to model dimers," J. Chem. Phys. **132**, 024505 (2010).

[29] L. Chen, R. Zheng, Y. Jing, and Q. Shi, "Simulation of the two-dimensional electronic spectra of the Fenna–Matthews–Olson complex using the hierarchical equations of motion method," J. Chem. Phys. **134**, 194508 (2011).

[30] A. Ishizaki and G. R. Fleming, "Unified treatment of quantum coherent and incoherent hopping dynamics in electronic energy transfer: Reduced hierarchy equation approach," J. Chem. Phys. **130**, 234111 (2009).

[31] D. Paleček, P. Edlund, E. Gustavsson, S. Westenhoff, and D. Zigmantas, "Potential pitfalls of the early-time dynamics in two-dimensional electronic spectroscopy," J. Chem. Phys. **151**, 024201 (2019).

[32] X. Leng, S. Yue, Y.-X. Weng, K. Song, and Q. Shi, "Effects of finite laser pulse width on two-dimensional electronic spectroscopy," Chem. Phys. Lett. **667**, 79–86 (2017).

[33] L. Seidner, G. Stock, and W. Domcke, "Nonperturbative approach to femtosecond spectroscopy: General theory and application to multidimensional nonadiabatic photoisomerization processes," J. Chem. Phys. **103**, 3998–4011 (1995).

[34] T. Mančal, A. V. Pisliakov, and G. R. Fleming, "Two-dimensional optical three-pulse photon echo spectroscopy. I. Nonperturbative approach to the calculation of spectra," J. Chem. Phys. **124**, 234504 (2006).

[35] P. Kjellberg and T. Pullerits, "Three-pulse photon echo of an excitonic dimer modeled via Redfield theory," J. Chem. Phys. **124**, 024106 (2006).

[36] A. Ishizaki and Y. Tanimura, "Nonperturbative non-Markovian quantum master equation: Validity and limitation to calculate nonlinear response functions," Chem. Phys. **347**, 185–193 (2008).

[37] M. F. Gelin, D. Egorova, and W. Domcke, "Efficient method for the calculation of time- and frequency-resolved four-wave mixing signals and its application to photon-echo spectroscopy," J. Chem. Phys. **123**, 164112 (2005).

[38] D. Egorova, M. F. Gelin, and W. Domcke, "Analysis of cross peaks in two-dimensional electronic photon-echo spectroscopy for simple models with vibrations and dissipation," J. Chem. Phys. **126**, 074314 (2007).

[39] Y.-C. Cheng, H. Lee, and G. R. Fleming, "Efficient simulation of three-pulse photon-echo signals with application to the determination of electronic coupling in a bacterial photosynthetic reaction center," J. Phys. Chem. A **111**, 9499–9508 (2007).

[40] Y.-C. Cheng, G. S. Engel, and G. R. Fleming, "Elucidation of population and coherence dynamics using cross-peaks in two-dimensional electronic spectroscopy," Chem. Phys. **341**, 285–295 (2007).

[41] Y.-C. Cheng and G. R. Fleming, "Coherence quantum beats in two-dimensional electronic spectroscopy," J. Phys. Chem. A **112**, 4254–4260 (2008).

[42] X. Leng, Y.-M. Yan, R.-D. Zhu, K. Song, Y.-X. Weng, and Q. Shi, "Simulation of the two-dimensional electronic spectroscopy and energy transfer dynamics of light-harvesting complex II at ambient temperature," J. Phys. Chem. B **122**, 4642–4652 (2018).

[43] X. Leng, T. N. Do, P. Akhtar, H. L. Nguyen, P. H. Lambrev, and H.-S. Tan, "Hierarchical equations of motion simulation of temperature-dependent two-dimensional electronic spectroscopy of the chlorophyll *a* manifold in LHCII," Chem. - Asian J. **15**, 1996–2004 (2020).

[44] J. Krčmář, M. F. Gelin, and W. Domcke, "Calculation of third-order signals via driven Schrödinger equations: General results and application to electronic 2D photon echo spectroscopy," Chem. Phys. **422**, 53–62 (2013).

[45] J. Wehner, M. Falge, W. T. Strunz, and V. Engel, "Quantum diffusion wave-function approach to two-dimensional vibronic spectroscopy," J. Chem. Phys. **141**, 134306 (2014).

[46] J. Albert, M. Falge, M. Keß, J. G. Wehner, P.-P. Zhang, A. Eisfeld, and V. Engel, "Extended quantum jump description of vibronic two-dimensional spectroscopy," J. Chem. Phys. **142**, 212440 (2015).

[47] J. M. Jackson, P. L. Brucia, and M. Messina, "An approach towards a simple quantum Langevin equation," Chem. Phys. Lett. **511**, 471–481 (2011).

[48] P. A. Brown and M. Messina, "Including memory friction in single- and two-state quantum dynamics simulations," J. Phys. Chem. B **120**, 1461–1475 (2016).

[49] N. G. Van Kampen, *Stochastic Processes in Physics and Chemistry* (Elsevier, 1992), Vol. 1.

[50] H.-P. Breuer, F. Petruccione *et al.*, *The Theory of Open Quantum Systems* (Oxford University Press on Demand, 2002).

[51] E. J. Heller, "Time-dependent approach to semiclassical dynamics," J. Chem. Phys. **62**, 1544–1555 (1975).

[52] E. J. Heller, "Classical *S*-matrix limit of wave packet dynamics," J. Chem. Phys. **65**, 4979–4989 (1976).

[53] G. W. Ford, J. T. Lewis, and R. F. O'Connell, "Quantum Langevin equation," Phys. Rev. A **37**, 4419–4428 (1988).

[54] R. Katz and P. B. Gossiaux, "The Schrodinger–Langevin equation with and without thermal fluctuations," Ann. Phys. **368**, 267–295 (2016).

[55] H. Peter and G.-L. Ingold, "Fundamental aspects of quantum Brownian motion," Chaos **15**(2), 026105 (2005).

[56] G. W. Ford, J. T. Lewis, and R. F. O'Connell, "Independent oscillator model of a heat bath: Exact diagonalization of the Hamiltonian," J. Stat. Phys. **53**, 439–455 (1988).

[57] J. M. Moix and J. Cao, "A hybrid stochastic hierarchy equations of motion approach to treat the low temperature dynamics of non-Markovian open quantum systems," J. Chem. Phys. **139**, 134106 (2013).

[58] X. Zhong, Y. Zhao, and J. Cao, "Coherent quantum transport in disordered systems: II. Temperature dependence of carrier diffusion coefficients from the time-dependent wavepacket diffusion method," New J. Phys. **16**, 045009 (2014).

[59] Y. Yan, Y. Liu, T. Xing, and Q. Shi, "Theoretical study of excitation energy transfer and nonlinear spectroscopy of photosynthetic light-harvesting complexes using the nonperturbative reduced dynamics method," Wiley Interdiscip. Rev.: Comput. Mol. Sci. **11**, e1498 (2020).

[60] M. H. Beck, A. Jäckle, G. A. Worth, and H.-D. Meyer, "The multiconfiguration time-dependent Hartree (MCTDH) method: A highly efficient algorithm for propagating wavepackets," Phys. Rep. **324**, 1–105 (2000).

[61] J. C. Light and T. Carrington, Jr., "Discrete-variable representations and their utilization," Adv. Chem. Phys. **114**, 263–310 (2000).